Ore Geology Reviews 90 (2017) 243–259

Contents lists available at ScienceDirect

Ore Geology Reviews

journal homepage: www.elsevier.com/locate/oregeo

Chemical homogeneity of high-Cr chromitites as indicator for widespread invasion of boninitic melt in mantle peridotite of Bir Tuluha ophiolite, Northern Arabian Shield, Saudi Arabia

Abdel Monem Habtoor [a], Ahmed Hassan Ahmed [a,b,*], Norikatsu Akizawa [c], Hesham Harbi [a], Shoji Arai [c]

[a] Faculty of Earth Sciences, King Abdulaziz University, Jeddah, Saudi Arabia
[b] Geology Department, Faculty of Science, Helwan University, Cairo, Egypt
[c] Department of Earth Sciences, Kanazawa University, Kanazawa 920-1192, Japan

ARTICLE INFO

Article history:
Received 27 July 2016
Received in revised form 4 March 2017
Accepted 10 March 2017
Available online 14 March 2017

Keywords:
Podiform chromitites
Chemical homogeneity
Chromian spinel
PGE-PGM
Bir Tuluha
Arabian Shield
Saudi Arabia

ABSTRACT

The Bir Tuluha ophiolite is one of the most famous chromitite-bearing occurrences in the Arabian Shield of Saudi Arabia, where chromitite bodies are widely distributed as lensoidal pods of variable sizes surrounded by dunite envelopes, and are both enclosed within the harzburgite host. The bulk-rock geochemistry of harzburgites and dunites is predominately characterized by extreme depletion in compatible trace elements that are not fluid mobile (e.g., Sr, Nb, Ta, Hf, Zr and heavy REE), but variable enrichment in the fluid-mobile elements (Rb and Ba). Harzburgites and dunites are also enriched in elements that have strong affinity for Mg and Cr such as Ni, Co and V. Chromian spinels in all the studied chromitite pods are of high-Cr variety; Cr-ratio (Cr/(Cr + Al) atomic ratio) show restricted range between 0.73 and 0.81. Chromian spinels of the dunite envelopes also show high Cr-ratio, but slightly lower than those in the chromitite pods (0.73–0.78). Chromian spinels in the harzburgite host show fairly lower Cr-ratio (0.49–0.57) than those in dunites and chromitites. Platinum-group elements (PGE) in chromitite pods generally exhibit steep negative slopes of typical ophiolitic chromitite PGE patterns; showing enrichment in IPGE (Os, Ir and Ru), over PPGE (Rh, Pt and Pd). The Bir Tuluha ophiolite is a unimodal type in terms of the presence of Ru-rich laurite, as the sole primary platinum-group minerals (PGM) in chromitite pods. These petrological features indicates that the Bir Tuluha ophiolite was initially generated from a mid-ocean ridge environment that produced the moderately refractory harzburgite, thereafter covered by a widespread homogeneous boninitic melt above supra-subduction zone setting, that produced the high-Cr chromitites and associated dunite envelopes. The Bir Tuluha ophiolite belt is mostly similar to the mantle section of the Proterozoic and Phanerozoic ophiolites, but it is a "unimodal" type in terms of high-Cr chromitites and PGE-PGM distribution.

1. Introduction

There are several lines of evidence for chemical heterogeneity in the Earth's upper mantle, during magma production and the subsequent recycling of the crustal rocks back into the mantle. The mantle heterogeneity can be displayed on a large scale, from the size of the ocean basin, to a minor scale, down to kilometer or even a meter scale (Hart et al., 1992; Liu et al., 2008). Both fertile and refractory mantle can be juxtaposed within the same area in the mantle lithosphere (Liu et al., 2008; Ahmed and Habtoor, 2015), which is used as a good indicator for second stage melting in forming a refractory boninitic melt above supra-subduction zone setting. Ophiolites are good windows of the mantle lithosphere exposed on the Earth's surface from which mantle heterogeneity can be examined. Ophiolites may be formed in a variety of tectonic settings, as indicated by the characteristic mineralogical and geochemical properties. They include fertile mantle (mid-ocean ridge (MOR)-related type) character, with Al-rich chromian spinels of relatively low Cr-ratio (Cr/(Cr + Al) < 0.6), and refractory mantle character (arc-related or supra-subduction zone (SSZ)-type) with Cr-rich chromian spinels of high Cr-ratio (>0.6) (Dick and Bullen, 1984; Zhou et al., 1998; Dare et al., 2009; Arai et al., 2011). Ophiolites contain significant podiform chromitite deposits hosted by harzburgites in the form of massive, nodular, banded, disseminated and orbicular occurrences. Chromian spinel, both in chromitites and/or in peridotites, occasionally survive alteration and can be

* Corresponding author at: Faculty of Earth Sciences, King Abdulaziz University, Jeddah, Saudi Arabia.
E-mail address: ahmh2jp@yahoo.com (A.H. Ahmed).

http://dx.doi.org/10.1016/j.oregeorev.2017.03.010
0169-1368/

used as a reliable petrogenetic indicator, even in highly serpentinized ultramafic rocks (Liipo et al., 1995; Ahmed et al., 2005). The primary chromian spinel chemistry provides important information about the composition of the parental melt (Rollinson, 2008), magmatic processes (partial melting) and fractional crystallization (Irvine, 1967; Roberts and Neary, 1993; Van der Veen and Maaskant, 1995), post cumulus stages variation in the physico-chemical conditions of parent magma (Ozawa, 1983; Leblanc and Ceuleneer, 1992; Zhou and Robinson, 1997; Krause et al., 2007) and subsolidus exolution or re-equilibration with co-existing phases (Jan et al., 1992; Krause et al., 2007; Ahmed et al., 2008). Platinum-group elements (PGE) are also important geochemical monitors of deep-seated mantle processes that provide information on the physico-chemical conditions and evolution of mantle lithosphere (Leblanc and Ceuleneer, 1992; Liipo et al., 1995; Ahmed and Arai, 2002; Ahmed et al., 2009).

Ophiolites are the oldest known oceanic fragments of the Arabian shield and adjoining regions, which are used to identify sutures between converging blocks of the lithosphere. The Arabian shield ophiolites are abundant as varyingly dismembered mafic–ultramafic assemblages that have suffered multiple phases of alteration, deformation and greenschist facies metamorphism (Al-Shanti and Gass, 1983; Nassief et al., 1984; Ahmed and Hariri, 2008). Limited detailed petrological studies on the ophiolitic upper mantle rocks (peridotites and associated chromitites) of the Arabian Shield concluded that the ophiolites of Saudi Arabia were possibly formed in a variety of tectonic settings, ranging from MOR to SSZ settings (Neary and Brown, 1979; Quick, 1990; Ahmed et al., 2012; Ahmed and Habtoor, 2015; Ahmed and Surour, 2016). The main chromitite-bearing ophiolitic upper mantle rocks in the Arabian Shield, arranged in a decreasing order of economic importance are: Al'Ays, Wadi Al Hwanet, Bir Tuluha, and Jabal Tays areas (Al-Shanti and El-Mahdy, 1988; Ahmed et al., 2012; Ahmed and Habtoor, 2015). Thus, podiform chromitites and associated peridotites of the Arabian Shield ophiolites can serve as markers of the mantle dynamics and deep-seated processes taking place beneath the Arabian Shield. Boninitic magma is widely considered as the dominant parental magma for podiform chromitite deposits in ophiolites, especially those of high-Cr varieties (Barnes and Röeder, 2001). The Bir Tuluha ophiolite belt is one of the most famous chromitite-bearing occurrences in the Arabian Shield of Saudi Arabia. Despite that, there exists no single petrological study describing geochemical and mineralogical characteristics of this important area. The present study represents the first detailed geochemical and mineralogical investigation of Bir Tuluha ophiolitic upper mantle rocks, including podiform chromitites and their host ultramafic rocks. The parental melt composition in equilibrium with the upper mantle rocks is calculated in order to deduce the tectonic setting and the style of melting regimes beneath the Arabian Shield during the formation of podiform chromitites. A comparison with other ophiolite complexes of older and younger ages worldwide is made to check the petrological similarity and/or differences during the Earth's history.

2. General geology and field setting

The Arabian Shield represents the exposed Precambrian basement of the Arabian Plate. It is exposed in the Western part of Saudi Arabia and in adjacent areas of Yemen and Jordan (Johnson, 1998). Stoeser and Camp (1985) divided the Arabian Shield into five geological terranes (microplates) bounded by four ophiolite-decorated sutures (Fig. 1a). The western terranes (Asir, Hijaz and Midyan) are separated by Bir Umq and Yanbu suture zones, and are composed of volcano-sedimentary sequences in ensimatic island arc environments (Stoeser and Camp, 1985; Stoeser and Stacey, 1988). The eastern terranes (Afif and Ar Rayn) have a continental affinity and join along the north-trending Al-Amar suture zone. From the viewpoint of age, the known mafic-ultramafic complexes in the Arabian Shield of Saudi Arabia are divided into two distinct groups: (1) Precambrian mafic-ultramafic complexes and, (2) mantle xenoliths enclosed in Tertiary mafic lavas (Harrat) associated with, and subsequently after, the opening of the Red Sea. The Precambrian mafic-ultramafic rock complexes in the Arabian shield are represented mainly by the ophiolite belts along suture zones, layered, and/or concentrically-zoned (Alaskan type) mafic–ultramafic intrusions (Fig. 1a). The ophiolites are found in various suture zones extended mainly in the N-S direction throughout the Arabian Shield (Fig. 1a). The upper mantle rocks of these ophiolite sequences are mainly serpentinized harzburgites and less abundant dunites. According to Al-Shanti and El-Mahdy (1988) and Stern et al. (2004), the ophiolite sequences in the Arabian Shield are divided into six belts (Fig. 1a): (1) Al Amar-Idsas belt: located in the eastern part of the Arabian Shield trending N–S, and associated with a profound suture zone known as Al Amar-Idsas Fault. (2) Jebel Humayyan-Jebel Sabhah belt: appearing to be parallel to Al Amar-Idsas belt. (3) Al Bijadiyah-Halaban belt: situated at the eastern margin of the Afif terrane. (4) Al Hulayfah-Hamdah (Nabitah) belt: trending N–S in the central part of the Arabian Shield within Najd Plateau. (5) Bir Umq-Jebel Thurwah belt: observed on a tectonic suture between Al-Hijaz terrane in the north and Jeddah terrane in the south. (6) Jebel Ess-Jebel Al Wasq belt: lying in the Northwestern part of the Arabian Shield, it separates Madyan terrane in the north from Al Hijaz terrane in the south.

The study area (Fig. 1a) lies approximately 250 km south of Hail in Northern Saudi Arabia, bounded by Longitude 40° 45′ and 40° 52′ E and Latitude 25° 33′ N and 25° 45′ N and 25 km south of the Al-Hulayfa town in the central part of the Arabian Shield. It is of low relief in the north and increases gradually to the south between Jabal Al Tin in the west and granite batholith in the east, which is characterized by ridges and high land (Fig. 1b). The rocks are strongly folded and sheared together with rocks of the Nuqrah formation. Layered metagabbro and younger fresh gabbro occur in a narrow band to the west and center of the study area, while diorite intrude the south and center parts of the ophiolite (Fig. 1b). The area also includes volcaniclastic rocks of the Hulayfah formation to the west, and bimodal basalt and rhyolite of the Shammar group and Shammar granites intrude in the eastern part (Fig. 1b). Minor coarse-grained amphibolite occurs in a narrow band to the center of the study area.

The ophiolite in Bir Tuluha is about 30 km long in the north-south direction and 6 km wide (Fig. 1b), parallel to the general strike of the stratified layered sequences in the area. The ultramafic rocks occur to the west of the area and are strongly serpenitinized and mylonitized, but harzburgite and dunite protoliths are still recognized. The study area is mostly flat-lying, with small mountains not exceeding few tens of meters high. Serpentinized harzburgite is the dominant rock type in the mantle section of the study area, while serpentinized dunite occurs as envelopes surrounding chromitite lenses, with variable thickness depending on the size of chromitite pods. Ultramafic rocks of Bir Tuluha ophiolite are highly sheared along the belt and completely altered to serpentinites, talc-carbonate and chlorite-bearing varieties.

Previous studies (Al-Shanti and El-Mahdy, 1988) reported the presence of 11 chromitite occurrences at Bir Tuluha area in different forms, including massive pods, layers, schlieren, *in situ* float boulders and mechanically displaced float boulders. Massive podiform chromitite lenses are mainly restricted to the northern-most part of Bir Tuluha ophiolite, where 6 chromitite pods are investigated in this study. Chromitite pods are trending generally in the N-S directions, forming prominent outcrops on the country rocks

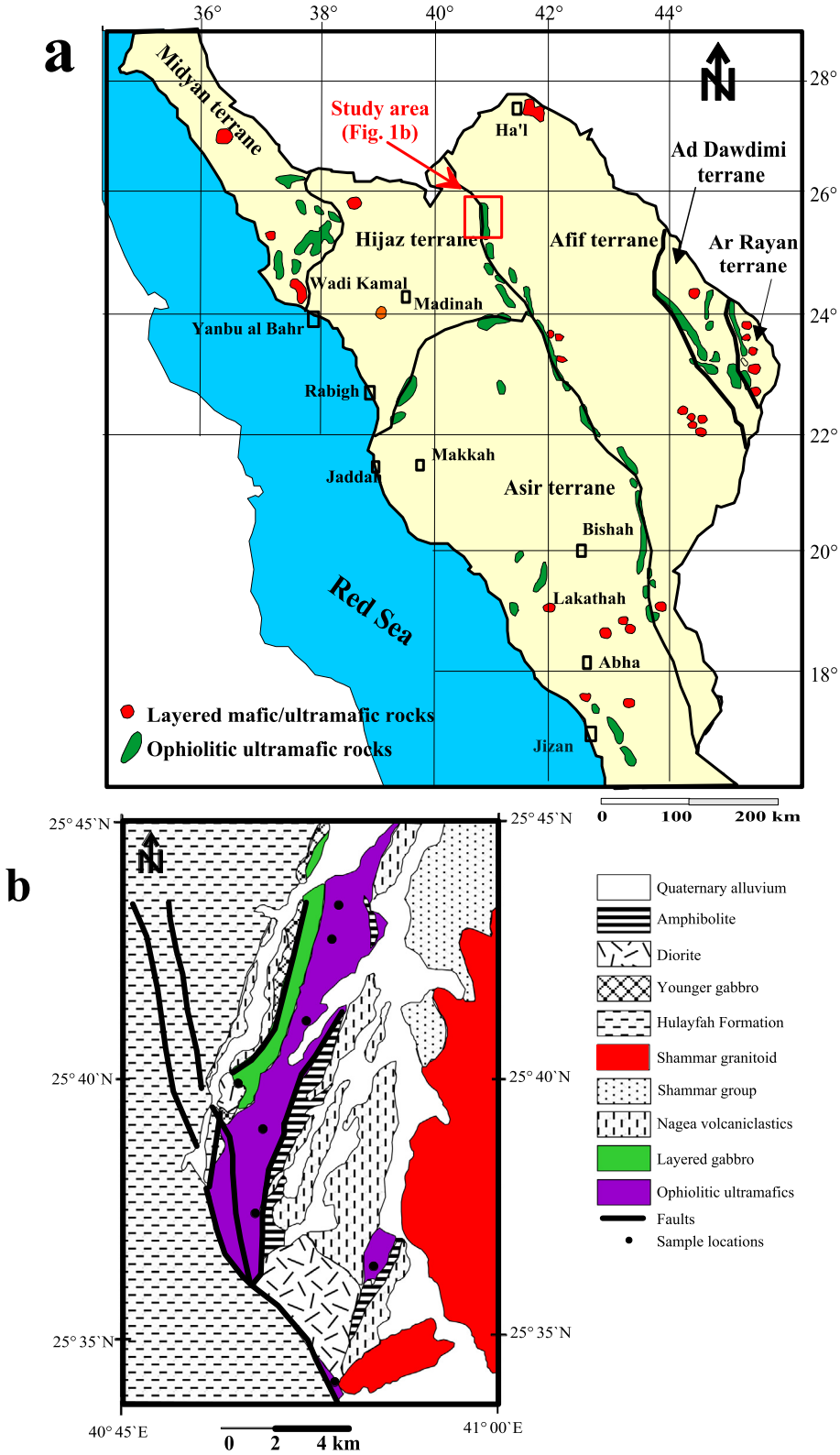

Fig. 1. (a) Map of the Arabian Shield showing the distribution of mafic-ultramafic rocks in the Kingdom of Saudi Arabia (modified from Collenette and Grainger (1994)). Location of the study areas is shown as red rectangle. (b) Simplified geological map of Bir Tuluha ophiolite (modified from Kattan (1983)). (For interpretation of the references to color in this figure legend, the reader is referred to the web version of this article.)

as a result of their greater resistance to weathering (Fig. 2a, b). The chromitite pods exhibit different shapes and sizes, ranging from elliptical to lenticular individual bodies (Fig. 2a), but sometimes occur as elongated bodies or boudinage (Fig. 2b). Regardless of the shape and size of chromitite pods, thin sheaths of serpentinized dunites, few tens of centimeters up to 2 m thick, envelope the chromitite lenses. All chromitite pods are concordant to the foliation in the surrounding serpentinized harzburgite. The chromitite

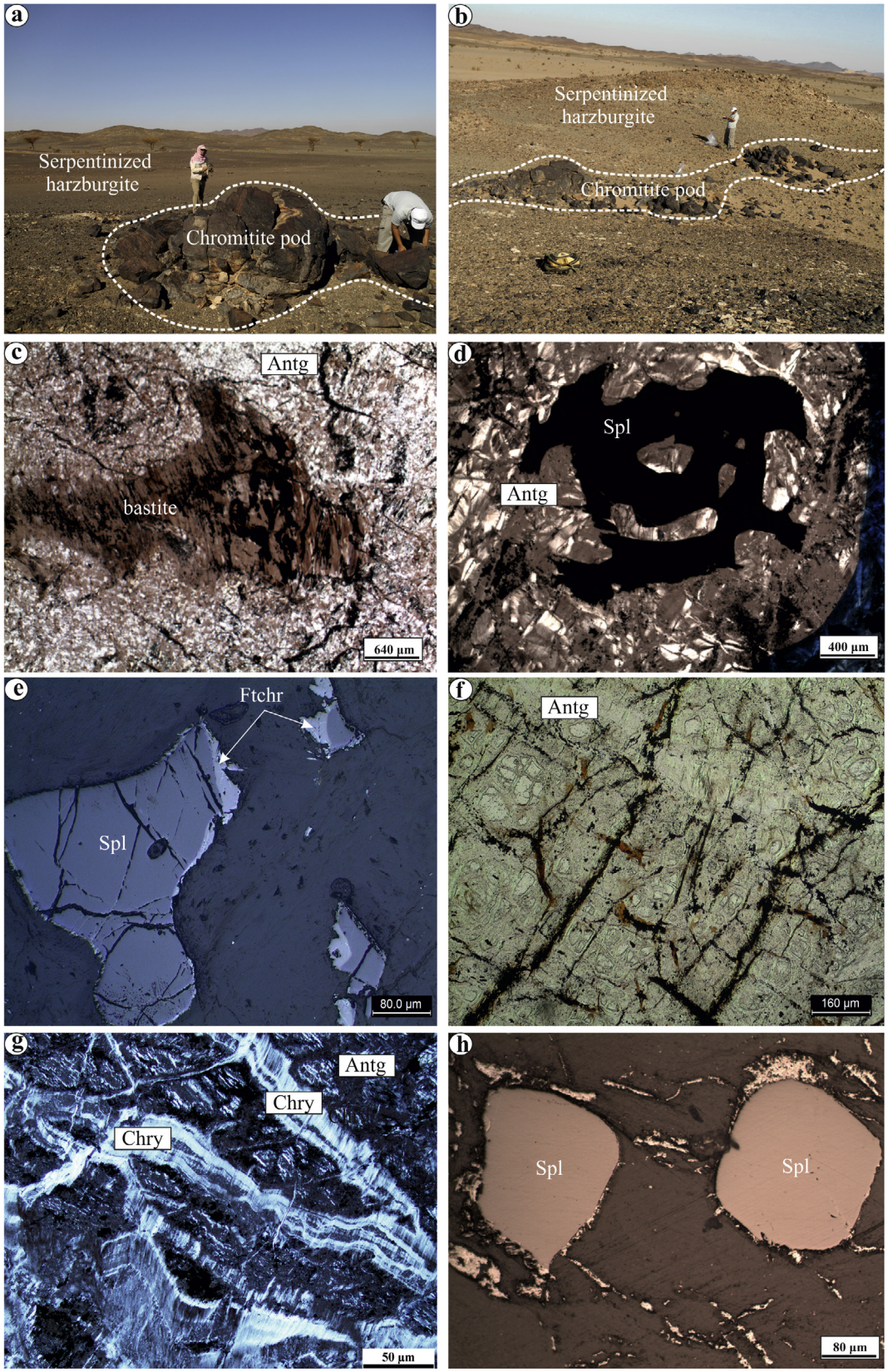

Fig. 2. (a) Field photo of individual fractured massive chromitite lens hosted by serpentinized harzburgite of Bir Tuluha ophiolite. (b) Field photo of small lensoidal chromitite pods forming boudinage structure hosted by serpentinized harzburgite. (c) Coarse-grained orthopyroxene pseudomorph completely altered to bastite in serpentinized harzburgite, plain polarized light (PPL). (d) Skeletal to vermicular chromian spinel (Spl) grain within serpentinized harzburgite, crossed-nicoles (CN). (e) Subhedral to anhedral chromian spinel partly altered to ferritchromite (Ftchr) along rims and cracks, reflected light (RL). (f) Pale green serpentinite showing mesh texture pseudomorphs after olivine of serpentinized dunite envelope. Magnetite (black lines and striations) filled the grain boundaries and cracks, PPL. (g) Fully serpentinized dunite envelope consisting of antigorite (Antg) and chrysotile (Chry) serpentine, CN. (h) Subhedral to euhedral fresh chromian spinel (Spl) in serpentinized dunite envelope, RL. (For interpretation of the references to color in this figure legend, the reader is referred to the web version of this article.)

lenses occur either as individual bodies or group of lenses, vary in length from 2 m to more than 10 m, and are up to 2 m thick (Fig. 2a, b).

3. Petrography

All ultramafic rocks of Bir Tuluha are highly serpentinized; all primary silicate minerals are completely altered to serpentines, carbonates and chlorite. Although the degree of serpentinization is high, the ultramafic protolith could be recognized as harzburgite by the bastite pseudomorphs, after orthopyroxene. Dunite envelopes around chromitite pods can be identified by its high shearing and partly by the mesh texture habit. Serpentinized harzburgite is medium-grained, black and sometimes dark greenish in color. Serpentine minerals are represented by antigorite and sometimes chrysotile and lizardite. The orthopyroxene pseudomorphs (bastite) are coarse-grained, with magnetite striations filling the cleavage planes of the original orthopyroxene crystals (Fig. 2c). Chromian spinels in harzburgite are mostly anhedral, amoeboid and skeletal in shape (Fig. 2d), which are weakly to moderately altered to ferritchromite (Fig. 2e). The serpentine minerals in dunite envelopes are mainly antigorite and sometimes chrysotile and lizardite, with characteristic mesh texture (Fig. 2f). Characteristic cross-fibers of chrysotile are also common in the dunite envelopes (Fig. 2g). Serpentinized dunite contains abundant disseminated euhedral to subhedral chromian spinel crystals (<4% rock volume), are usually weakly altered and fractured than those in the serpentinized harzburgite (Fig. 2h).

All chromitite pods in Bir Tuluha are mainly massive and composed of more than 90% modal chromian spinel crystals. Massive chromitite is generally black and coarse-grained on the fresh surface. In thin sections, chromitite is composed of granular aggregates of coarse-grained (up to 10 mm) chromian spinel that have a closely packed fabric, interlocking grains contain a variable quantity (<10%) of interstitial silicate minerals. The chromian spinel crystals are of various shapes; the most common are sub rounded spherical, oval, polygonal, and irregular (Fig. 3a). Due to its brittleness, chromian spinels are firstly affected by tectonic disturbances through slight fracturing thus forming a network of irregular cracks; these fractures are occasionally filled with gangue silicates. Brecciation commonly affects the massive chromian spinel that is located near the shearing planes and along fracture zones. In the brecciated chromian spinel, the grains are broken along the fractures forming a characteristic cataclastic texture (Fig. 3a). Chromian spinel sometimes contains inclusions of silicate minerals that are spherical to euhedral in shape, and are mostly of altered olivine and orthopyroxene that range in size from several μm to about 100 μm (Fig. 3b). Silicate mineral inclusions are often altered to serpentine and chlorite minerals. Chromian spinels of chromitite pods are slightly affected by serpentinization and post-magmatic processes; the ferritchromite and Cr-rich magnetite rims are very rare, which are focused on the periphery and along fractures of chromian spinel grains. Eleven grains of platinum-group minerals (PGM) were found among the 15 thin polished sections of the studied chromitite samples. These either as solitary inclusions within chromian spinel (Fig. 3c), or within the matrix of brecciated chromian spinel (Fig. 3d). They are mainly euhedral polygonal crystals with sizes ranging from 10 to 40 μm across (Fig. 3c and d). Laurite (RuS2) is the only PGM phase observed in the studied chromitite pods.

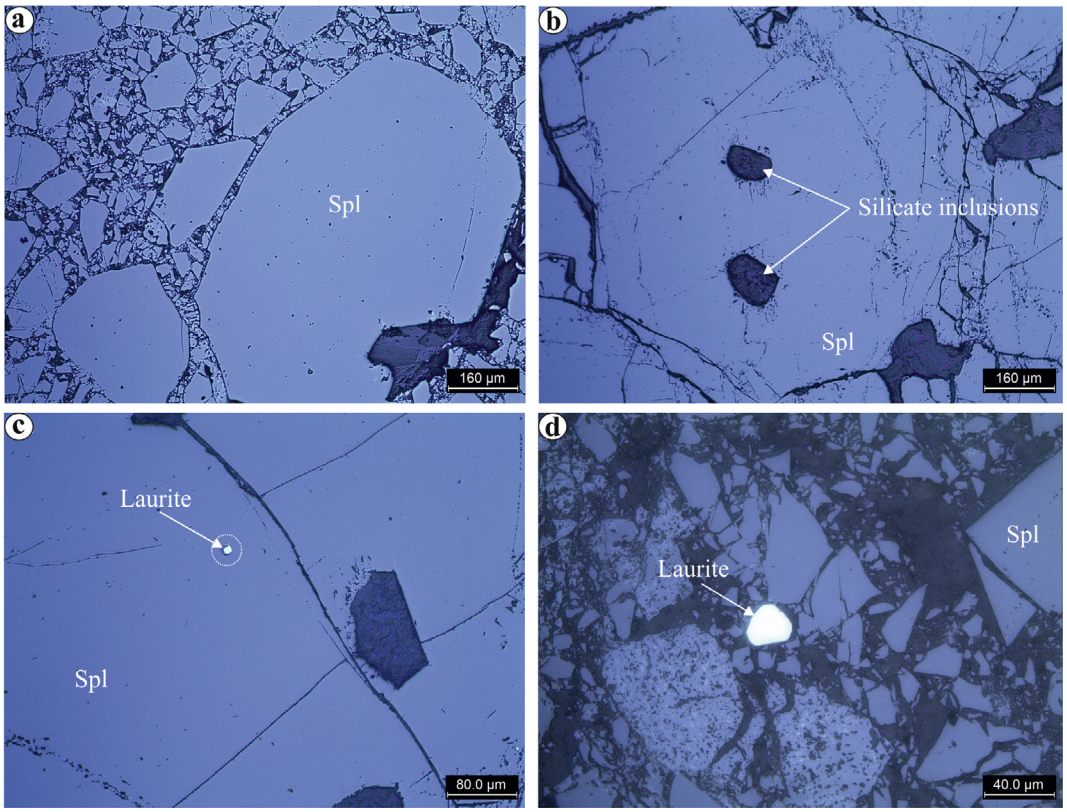

Fig. 3. Photomicrographs of chromitite pods in Bir Tuluha ophiolite belt. (a) Coarse-grained chromian spinels (Spl) partly brecciated and cracked showing polygonal, and irregular crystal edges, in the massive chromitite, RL. (b) Altered silicate mineral inclusions in fresh, cracked chromian spinel in massive chromitite, RL. (c) Euhedral platinum-group mineral grain (laurite) within fresh chromian spinel of chromitites, RL. (d) Polygonal euhedral laurite grain within the interstitial matrix of brecciated chromian spinels of massive chromitite, RL.

4. Geochemistry

4.1. Analytical techniques

Representative samples from Bir Tuluha serpentinized harzburgites, dunites and chromitites have been analyzed for their major, trace and rare-earth element (REE) composition. The bulk rock analysis was performed on 0.2 g samples using inductively coupled plasma-mass spectrometry (ICP-MS), following a $LiBO_2$ fusion and diluted nitric acid digestion. All analyses were carried out in the ACME analytical laboratories, Canada. Table 1 shows the data for major and some detectable trace elements. Almost all REE are below the detection limits, that is why they are not included in the data of Table 1. The bulk rock samples are also analyzed for total platinum-group elements (PGE) and Au contents using the 9000 ICP-MS after fire assay techniques at the Genalysis Laboratory Services Pty. Ltd., Maddington, Western Australia. Laboratory standards were used for instrument calibration and drift correction. Analytical accuracy and precision were routinely checked using international standards, and by analyzing blanks and duplicates. Detection limits were 1 ppb for all PGE except Au, which is 2 ppb. The PGE contents of the analyzed samples are listed in Table 2.

Mineral chemistry of silicates and oxides in all rock types was carried out using a JEOL electron-probe micro analyzer (EPMA) JXA-8800 at the Center for Cooperative Research of Kanazawa University, Japan. Analytical conditions were: 20 kV accelerating voltage, 15 nA probe current and 3 μm beam diameter. The raw

Table 1
Bulk-rock geochemistry of Bir Tuluha serpentinized harzburgite, dunite and chromitite. Detection limit (DL) for all major oxides is (0.01 wt%) while the DL of trace elements (ppm) is between brackets.

Rock type	Serpentinized dunite		Serpentinized harzburgite		Chromitite				
Sample	3	D2	O1	O2	P2a	P4a	P5a	P5b	C3
SiO_2	39.18	38.81	40.76	40.61	2.02	4.2	4.44	3.43	3.87
Al_2O_3	0.41	0.47	0.64	0.47	13.21	9.59	10.31	10.52	8.07
Fe_2O_3	8.93	9.26	7.06	6.86	14.62	15.09	14.87	14.66	15.28
CaO	0.1	0.15	0.18	0.14	0.23	0.02	0.01	0.01	0.96
MgO	38.38	38.8	38.94	39.02	15.57	16.55	17.02	16.36	15.9
Na_2O	0.01	0.01	0.01	0.01	0.01	0.01	0.01	0.01	0.01
K_2O	0.01	0.01	0.01	0.01	0.01	0.01	0.01	0.01	0.01
MnO	0.1	0.11	0.07	0.08	0.14	0.64	0.37	0.29	0.17
TiO_2	0.01	0.01	0.01	0.01	0.12	0.11	0.1	0.15	0.09
P_2O_5	0.01	0.01	0.01	0.01	0.01	0.01	0.01	0.01	0.01
Cr_2O_3	1.556	0.689	0.357	0.386	53.136	52.518	52.65	54.117	55.853
LOI	12.42	12.6	12.88	12.94	0.55	0.87	1.32	1.28	0.85
Total	101.08	100.88	100.89	100.51	99.56	99.56	101.08	100.78	100.99
TOT/C	0.03	0.05	0.03	0.03	0.02	0.02	0.02	0.02	0.02
TOT/S	0.02	0.02	0.02	0.02	0.02	0.02	0.02	0.02	0.02
Trace elements (ppm)									
Ba (1)	14	4	14	53	1	8	2	6	8
Co (0.2)	122.6	104.2	94.4	97.2	67.5	73.6	75.3	85.2	73.4
Ga (0.5)	0.5	0.5	0.5	0.5	11.6	10.4	11.5	12.6	7.7
Hf (0.1)	0.1	0.1	0.1	0.1	0.1	0.1	0.1	0.1	0.1
Nb (0.1)	0.1	0.1	0.1	0.1	0.1	0.1	0.1	0.1	0.1
Rb (0.1)	0.1	0.1	0.4	0.1	1.6	2	2.2	2.1	2.4
Sr (0.5)	7.3	4.2	19.3	13.2	2	1.9	1.1	1.8	2.1
Ta (0.1)	0.1	0.1	0.1	0.1	0.1	0.1	0.1	0.1	0.1
Th (0.2)	0.2	0.2	0.2	0.2	0.2	0.2	0.2	0.2	0.2
U (0.1)	0.1	0.1	0.1	0.1	0.1	0.1	0.1	0.1	0.1
V (8)	18	21	37	27	445	424	424	479	244
W (0.5)	1.9	1.3	2.4	2.1	65.1	46.2	25.6	56.8	56.2
Zr (0.1)	0.6	0.3	0.1	0.2	1.1	0.7	0.7	0.6	0.5
Mo (0.1)	0.1	0.1	0.1	0.2	0.1	0.1	0.1	0.3	0.1
Cu (0.1)	12.6	2.1	12.2	3.3	1.7	2.3	0.9	4.7	3
Pb (0.1)	0.1	0.1	0.8	0.3	0.1	0.1	0.1	0.1	0.1
Zn (1)	27	30	17	23	1	17	4	2	1
Ni (0.1)	2790	1412	2270	2252	196	223	192	233	431

Table 2
Whole rock geochemistry of platinum-group elements (in ppb) in chromitites, dunites and harzburgite of Bir Tuluha ophiolite.

Rock type	Dunite envelopes		Harzburgite host		Chromitites				
Sample No.	3	D2	O1	O2	P2a	P4a	P5a	P5b	C3
Ir	1	1	3	4	45	33	37	34	35
Os	1	1	3	4	56	14	19	41	37
Ru	3	2	6	7	103	80	83	97	91
Rh	1	2	1	2	6	8	9	9	9
Pd	1	1	8	1	2	1	5	1	5
Pt	4	3	6	7	5	6	8	7	3
Total PGE	11	10	27	25	217	142	161	189	180
Pd/Ir	1	1	2.67	0.25	0.04	0.03	0.14	0.03	0.14
Ru/Pt	0.75	0.67	1	1	20.6	13.33	10.38	13.86	30.33

Table 3
Representative microprobe analyses of chromian spinels in serpentinized dunites and harzburgites of Bir Tuluha ophiolite. Fe+3-ratio: Fe3+/(Fe3+ + Al + Cr) atomic ratio, Cr-ratio: Cr/(Cr + Al), atomic ratio, Mg-ratio: Mg/(Mg + Fe2+) atomic ratio. n.d. = not detected.

Rock Type	Dunite envelopes				Harzburgite host							
Sample	2				H3				O1			
SiO_2	0.07	0.23	0.25	0.05	n.d.	0.01	n.d.	n.d.	0.02	n.d.	0.02	n.d.
TiO_2	0.25	0.22	0.24	0.22	0.03	0.04	0.02	n.d.	0.06	0.03	0.07	0.06
Al_2O_3	11.61	12.00	13.07	10.78	23.62	26.25	24.65	23.25	27.17	28.06	27.57	26.81
Cr_2O_3	56.26	56.00	53.64	57.75	45.36	41.28	43.98	45.93	40.69	40.35	42.85	42.87
FeO*	22.35	22.03	22.73	21.32	17.95	20.40	17.89	17.07	17.97	18.41	14.95	15.61
MnO	0.36	0.32	0.32	0.31	0.26	0.25	0.25	0.23	0.23	0.24	0.24	0.24
MgO	10.90	11.06	10.67	11.41	13.46	12.79	13.68	13.67	13.82	13.97	15.48	15.06
CaO	n.d.	0.01	0.03	n.d.	n.d.	n.d.	n.d.	n.d.	n.d.	n.d.	n.d.	n.d.
Na_2O	n.d.	n.d.	n.d.	0.01	n.d.	n.d.	n.d.	n.d.	n.d.	n.d.	0.03	n.d.
K_2O	n.d.	n.d.	0.01	n.d.	0.01	n.d.	n.d.	n.d.	n.d.	n.d.	0.01	n.d.
NiO	0.11	0.09	0.10	0.07	0.06	0.07	0.09	0.09	0.11	0.10	0.07	0.12
Total	101.90	101.95	101.04	101.92	100.76	101.07	100.56	100.23	100.07	101.17	101.28	100.76
Oxygen atoms	4	4	4	4	4	4	4	4	4	4	4	4
Si	0.002	0.007	0.008	0.002	0.000	0.000	0.000	0.000	0.001	0.000	0.001	0.000
Ti	0.006	0.005	0.006	0.005	0.001	0.001	0.000	0.000	0.001	0.001	0.002	0.001
Al	0.445	0.458	0.502	0.413	0.851	0.939	0.885	0.840	0.968	0.987	0.959	0.943
Cr	1.446	1.432	1.381	1.483	1.095	0.990	1.058	1.113	0.972	0.952	0.999	1.011
Fe^*	0.608	0.596	0.619	0.579	0.459	0.518	0.456	0.438	0.454	0.460	0.369	0.389
Fe^{2+}	0.480	0.473	0.488	0.456	0.395	0.432	0.388	0.383	0.384	0.387	0.323	0.336
Fe^{3+}	0.125	0.121	0.129	0.121	0.069	0.091	0.074	0.061	0.073	0.077	0.049	0.057
Mn	0.010	0.009	0.009	0.009	0.007	0.006	0.006	0.006	0.006	0.006	0.006	0.006
Mg	0.528	0.533	0.518	0.553	0.613	0.579	0.621	0.625	0.623	0.622	0.681	0.669
Ca	0.000	0.000	0.001	0.000	0.000	0.000	0.000	0.000	0.000	0.000	0.000	0.000
Na	0.000	0.000	0.000	0.001	0.000	0.000	0.000	0.000	0.000	0.000	0.002	0.000
K	0.000	0.000	0.000	0.000	0.000	0.000	0.000	0.000	0.000	0.000	0.000	0.000
Ni	0.002	0.002	0.002	0.001	0.001	0.001	0.002	0.002	0.002	0.002	0.001	0.002
Total	3.044	3.041	3.042	3.043	3.032	3.039	3.034	3.029	3.031	3.034	3.022	3.026
Fe^{2+}	0.48	0.47	0.48	0.45	0.39	0.43	0.38	0.38	0.38	0.38	0.32	0.33
Fe^{3+}-ratio	0.06	0.06	0.06	0.06	0.03	0.05	0.04	0.03	0.04	0.04	0.02	0.03
Mg-ratio	0.52	0.53	0.52	0.55	0.61	0.57	0.62	0.62	0.62	0.62	0.68	0.67
Cr-ratio	0.76	0.76	0.73	0.78	0.56	0.51	0.54	0.57	0.50	0.49	0.51	0.52

data were corrected with an online ZAF correction program. The amounts of Fe^{3+} and Fe^{2+} in chromian spinel were calculated with the assumption of spinel stoichiometry. Selected microprobe analyses of the analyzed minerals are presented in Tables 3–5. Quantitative analysis of PGM grains was carried out using two EPMA laboratories; JEOL JXA-8800 at the Center for Cooperative Research of Kanazawa University, Japan, and JEOL JXA-8200 at the Department of Mineral Resources and Rocks of the Faculty of Earth Sciences, King Abdulaziz University, Jeddah, Saudi Arabia. Analytical conditions in both laboratories were: 25 kV accelerating voltage and 20 nA probe current. Standards used were pure metals for the elements Os, Ir, Ru, Rh, Pt, Pd, Cu, and Cr, gallium arsenide for As, and pentlandite for S, Fe and Ni. The Kα X-ray lines were used for Ni, S, Fe, and Cr, Lα lines for Os, Ir, Ru, Rh, Pt and Cu, and Lβ lines for Pd and As. The microprobe analyses of PGM grains are listed in Table 5.

4.2. Bulk-rock geochemistry

4.2.1. Major elements

Whole-rock major oxides of serpentinized harzburgites, dunites, and chromitites from the Bir Tuluha ophiolite are given in Table 1. The serpentinized harzburgites and dunites show more or less comparable major oxides composition (Table 1). The low SiO_2 and CaO contents in harzburgites and dunites suggest that silicification and carbonation processes are basically low and serpentinization is the main alteration process. Loss-on-ignition (LOI) values (12.4–12.94%) also indicate that both dunites and harzburgites were highly hydrated (serpentinized). In the analyzed chromitite samples, the Cr_2O_3 content is very restricted around the high-Cr varieties, with ranges from 52.59 to 55.86 wt% (average 53.2 wt%). The other major oxides in chromitites also vary within narrow ranges (average of MgO, Al_2O_3 and Fe_2O_3 are 16.28 wt%, 10.34 wt%, and 14.9 wt%, respectively) (Table 1).

4.2.2. Trace and REE geochemistry

The serpentinized harzburgites and dunites are characterized by relatively high concentrations of compatible trace elements which have a strong affinity for Mg and Cr, such as Ni, Co and V, while they generally have low concentrations of incompatible elements (Table 1). Chromitite samples have lower Ni and Co contents, but higher V content, compared with those in dunites and harzburgites (Table 1). In the N-MORB normalized spider diagram (Fig. 4), the harzburgites and dunites show comparable patterns; they are highly depleted in Sr, Nb, Hf and Zr, and relatively enriched in the fluid-mobile large ion lithophile elements (LILE), such as Rb and Ba (Fig. 4). The REE contents are generally very low in all the studied samples (Table 1), which is a general feature of the ophiolitic mantle rocks (Johnson and Fryer, 1990); almost all the REE are below the detection limits. Hence, the REE contents and patterns are not included in this study.

4.3. Platinum-group elements geochemistry (PGE)

The PGE analyses for the Bir Tuluha harzburgites, dunites, and chromitites are presented in Table 2. In general, serpentinized harzburgites and dunites have much lower PGE contents relative to the associated chromitite pods. Their PGE show flat or nearly unfractionated patterns; mostly similar to the average mantle PGE contents and patterns (Fig. 5a), where the Pd/Ir ratio is almost around unity. The PGE contents in dunite envelopes are relatively lower than those in the harzburgite host, which might be due to

Table 4
Representative microprobe analyses of chromian spinels in chromitite pods of Bir Tuluha ophiolite. Cr-ratio: Cr/(Cr + Al), atomic ratio, Fe+3-ratio: Fe3+/(Fe3+ + Al + Cr), atomic ratio, Mg-ratio: Mg/(Mg + Fe2+) atomic ratio. n.d. = not detected.

Rock Type	Chromitite																			
Sample	C3				P1				P4b				P5b				P5a			
SiO_2	n.d.	0.91	0.003	n.d.	n.d.	n.d.	n.d.	n.d.	0.028	n.d.	n.d.	n.d.	0.001	0.009	n.d.	n.d.	n.d.	n.d.	n.d.	n.d.
TiO_2	0.11	0.09	0.09	0.14	0.10	0.11	0.12	0.10	0.11	0.11	0.11	0.11	0.14	0.15	0.11	0.095	0.10	0.16	0.11	0.15
Al_2O_3	10.40	9.68	10.19	10.49	14.17	13.99	14.94	15.04	11.76	11.39	12.17	11.60	12.36	12.67	12.04	11.66	12.29	12.89	11.87	12.33
Cr_2O_3	61.66	60.81	61.05	61.38	57.28	57.81	56.91	57.15	60.41	60.98	60.01	60.46	60.78	59.92	60.99	60.255	60.50	59.73	60.86	60.22
FeO*	13.10	12.99	12.18	13.48	12.51	12.66	13.61	13.56	13.87	12.19	12.28	13.02	12.12	12.07	12.10	13.534	13.34	12.12	12.77	13.38
MnO	0.15	0.19	0.23	0.21	0.21	0.20	0.20	0.23	0.21	0.19	0.22	0.24	0.27	0.22	0.20	0.24	0.27	0.26	0.21	0.21
MgO	16.06	15.71	16.08	15.98	15.38	15.63	15.45	15.72	15.40	15.13	15.20	14.66	14.84	15.12	14.90	14.826	15.77	15.83	15.92	15.72
CaO	n.d.	0.24	n.d.	n.d.	n.d.	n.d.	n.d.	n.d.	n.d.	n.d.	n.d.	n.d.	n.d.	n.d.	n.d.	n.d.	n.d.	n.d.	n.d.	n.d.
Na_2O	n.d.	n.d.	n.d.	n.d.	n.d.	n.d.	n.d.	n.d.	n.d.	n.d.	n.d.	n.d.	n.d.	n.d.	n.d.	n.d.	n.d.	n.d.	n.d.	n.d.
K_2O	n.d.	n.d.	n.d.	n.d.	n.d.	n.d.	n.d.	n.d.	n.d.	n.d.	n.d.	0.011	0.007	n.d.	n.d.	0.003	n.d.	n.d.	n.d.	n.d.
NiO	0.13	0.15	0.16	0.12	0.18	0.15	0.15	0.15	0.16	0.13	0.13	0.13	0.18	0.16	0.20	0.125	0.17	0.18	0.20	0.16
Total	101.61	100.75	99.97	101.79	99.83	100.56	101.37	101.96	101.95	100.11	100.12	100.25	100.69	100.32	100.52	100.74	102.43	101.17	101.93	102.17
Oxygen atoms	4	4	4	4	4	4	4	4	4	4	4	4	4	4	4	4	4	4	4	4
Si	0.000	0.029	0.000	0.000	0.000	0.000	0.000	0.000	0.001	0.000	0.000	0.000	0.000	0.000	0.000	0.000	0.000	0.000	0.000	0.000
Ti	0.003	0.002	0.002	0.003	0.002	0.002	0.003	0.002	0.002	0.003	0.003	0.003	0.003	0.003	0.003	0.002	0.002	0.004	0.002	0.003
Al	0.387	0.362	0.388	0.390	0.551	0.543	0.547	0.547	0.435	0.422	0.449	0.430	0.451	0.463	0.441	0.462	0.450	0.472	0.437	0.453
Cr	1.538	1.527	1.538	1.530	1.395	1.404	1.398	1.395	1.498	1.515	1.486	1.504	1.489	1.469	1.498	1.475	1.488	1.467	1.503	1.484
Fe*	0.346	0.345	0.346	0.355	0.348	0.351	0.354	0.350	0.364	0.373	0.374	0.395	0.340	0.339	0.340	0.351	0.347	0.341	0.334	0.349
Fe^{2+}	0.253	0.249	0.257	0.257	0.285	0.289	0.289	0.283	0.286	0.297	0.297	0.319	0.273	0.260	0.269	0.276	0.275	0.271	0.264	0.274
Fe^{3+}	0.092	0.096	0.090	0.097	0.064	0.062	0.064	0.069	0.079	0.076	0.078	0.078	0.068	0.078	0.071	0.076	0.074	0.069	0.070	0.073
Mn	0.004	0.005	0.006	0.006	0.006	0.005	0.005	0.006	0.006	0.005	0.006	0.007	0.007	0.006	0.005	0.006	0.007	0.007	0.006	0.005
Mg	0.755	0.743	0.751	0.751	0.720	0.716	0.715	0.723	0.720	0.709	0.709	0.688	0.732	0.745	0.736	0.730	0.731	0.733	0.741	0.730
Ca	0.000	0.008	0.000	0.000	0.000	0.000	0.000	0.000	0.000	0.000	0.000	0.000	0.000	0.000	0.000	0.000	0.000	0.000	0.000	0.000
Na	0.000	0.000	0.000	0.000	0.000	0.000	0.000	0.000	0.000	0.000	0.000	0.000	0.000	0.000	0.000	0.000	0.000	0.000	0.000	0.000
K	0.000	0.000	0.000	0.000	0.000	0.000	0.000	0.000	0.000	0.000	0.000	0.000	0.000	0.000	0.000	0.000	0.000	0.000	0.000	0.000
Ni	0.003	0.003	0.003	0.003	0.004	0.003	0.003	0.003	0.003	0.003	0.003	0.003	0.004	0.003	0.004	0.003	0.004	0.004	0.004	0.003
Total	3.034	3.025	3.036	3.036	3.025	3.024	3.025	3.028	3.031	3.029	3.030	3.031	3.027	3.029	3.028	3.031	3.031	3.026	3.028	3.027
Fe^{2+}	0.25	0.25	0.25	0.26	0.28	0.29	0.29	0.28	0.28	0.30	0.30	0.32	0.27	0.26	0.27	0.27	0.27	0.27	0.26	0.27
Fe^{3+}-ratio	0.05	0.05	0.04	0.05	0.03	0.03	0.03	0.03	0.04	0.04	0.04	0.04	0.03	0.04	0.04	0.04	0.04	0.03	0.03	0.04
Mg-ratio	0.75	0.75	0.75	0.74	0.72	0.71	0.71	0.72	0.72	0.70	0.70	0.68	0.73	0.74	0.73	0.73	0.73	0.73	0.74	0.73
Cr-ratio	0.80	0.81	0.80	0.80	0.72	0.72	0.72	0.72	0.78	0.78	0.77	0.78	0.77	0.76	0.77	0.76	0.77	0.76	0.77	0.77

Table 5
Microprobe analyses of laurite in chromitites from Bir Tuluha ophiolite. n.d. = not detected. Ru ratio = Ru/(Ru + Os + Ir).

Sample	1-Core	1-Rim	2-Core	2-Rim	3-Core	3-Rim	4-Core	4-Rim	5	6	7	8	9	10	11-Core	11-Rim
S	36.46	36.97	37.09	37.08	36.42	38.54	36.16	39.69	37.86	37.15	37.75	35.16	35.84	38.74	37.52	34.06
Os	5.86	5.49	3.79	1.59	4.17	2.00	1.87	1.00	1.85	2.00	1.25	0.42	2.31	3.47	2.82	1.51
Ir	1.34	1.19	3.03	1.79	4.07	2.56	3.65	2.78	4.42	2.66	1.52	2.59	1.56	3.19	4.48	6.21
Ru	52.82	52.17	52.31	54.94	51.43	55.44	53.75	54.75	54.89	54.79	54.68	51.25	51.70	48.97	51.86	50.25
Rh	0.84	0.95	1.10	1.42	1.56	1.28	1.42	1.20	1.25	1.15	2.45	1.53	2.55	1.82	2.17	2.60
Pt	n.d.	n.d.	n.d.	0.25	n.d.	n.d.	n.d.	n.d.	n.d.	n.d.	n.d.	0.24	0.06	0.31	n.d.	n.d.
Pd	n.d.	0.10	n.d.	0.12	0.02	n.d.	0.28	n.d.	0.43	0.11	0.30	2.43	1.67	2.00	2.14	2.08
Ni	n.d.	0.01	0.44	0.33	0.38	0.05	0.13	0.05	0.04	0.05	0.09	0.75	0.10	n.d.	n.d.	0.03
Fe	1.50	1.19	0.64	0.46	0.49	0.35	0.18	0.22	0.24	1.13	0.53	1.40	1.06	0.43	0.18	0.62
Cr	2.59	3.71	1.17	1.01	1.08	1.16	0.73	0.82	0.89	1.94	0.72	3.58	2.52	1.75	0.47	2.78
Total	101.41	101.77	99.55	99.00	99.61	101.37	98.15	100.51	101.87	100.98	99.28	99.36	99.36	100.66	101.64	100.13
Ru ratio	0.88	0.89	0.88	0.94	0.86	0.92	0.91	0.94	0.90	0.92	0.95	0.94	0.93	0.88	0.88	0.87
Atomic%																
S	63.81	63.80	65.65	65.44	65.32	66.19	65.41	67.59	65.79	64.53	65.99	62.13	63.54	66.87	65.94	62.15
Os	1.73	1.60	1.13	0.47	1.26	0.58	0.57	0.29	0.54	0.59	0.37	0.12	0.69	1.01	0.84	0.47
Ir	0.39	0.34	0.89	0.53	1.22	0.73	1.10	0.79	1.28	0.77	0.44	0.76	0.46	0.92	1.31	1.89
Ru	29.32	28.56	29.37	30.75	29.26	30.20	30.84	29.57	30.25	30.19	30.32	28.72	29.07	26.81	28.91	29.08
Rh	0.46	0.51	0.61	0.78	0.87	0.68	0.80	0.64	0.67	0.62	1.33	0.84	1.41	0.98	1.19	1.48
Pt	–	–	–	0.07	–	–	–	–	–	–	–	0.07	0.02	0.09	–	–
Pd	–	0.05	–	0.06	0.01	–	0.15	–	0.23	0.06	0.16	1.30	0.89	1.04	1.13	1.14
Ni	–	0.01	0.42	0.32	0.37	0.04	0.12	0.04	0.04	0.05	0.08	0.73	0.10	–	–	0.02
Fe	1.51	1.18	0.65	0.47	0.50	0.34	0.19	0.21	0.24	1.12	0.53	1.42	1.07	0.42	0.18	0.64
Cr	2.79	3.95	1.28	1.09	1.19	1.23	0.81	0.86	0.96	2.08	0.77	3.90	2.75	1.86	0.51	3.13

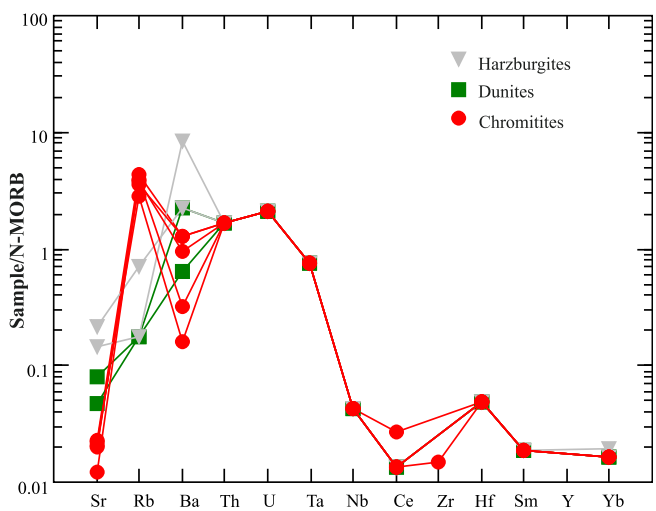

Fig. 4. N-MORB normalized spider diagrams of the chromitites, serpentinized dunites and harzburgites of the Bir Tuluha ophiolite (normalization values are from McDonough and Sun, 1989).

the close association with the chromitite pods which collect the PGE from the melt. The obvious positive Rh anomaly of one dunite sample is most probably due to the nugget effect. The PGE concentrations in the chromitites of Bir Tuluha ophiolite are comparable with those from podiform chromitites of ophiolites worldwide (Fig. 5b). The total PGE contents vary from 142 to 217 ppb, with an average of 178 ppb (Table 2). All the chromitite samples from the Bir Tuluha ophiolite display a steep negative slope from Ru to Pd in the PGE spider diagrams; being highly enriched in IPGE (Os, Ir and Ru) and extremely depleted in PPGE (Rh, Pt and Pd) (Fig. 5b). The Ru/Pt fractionation ratio is remarkably high, varying from 10 to 30, with an average of 20, and the Pd/Ir ratio, one of the best indicators for PGE fractionation, is very low, from 0.03 to 0.14, mostly similar to those from the PGE-rich chromitites of the Oman ophiolite (Ahmed and Arai, 2002). The studied chromitite pods are entirely overlapped with those from the Proterozoic ophiolites of Egypt, Morocco, Saudi Arabia (Ahmed, 2013; Ahmed et al., 2009, 2012; Ahmed and Habtoor, 2015), and Phanerozoic ophiolite of Oman (Ahmed and Arai, 2002) (Fig. 5b).

5. Mineral chemistry

5.1. Chromian spinel

Representative analyses of chromian spinels from the chromitite pods and serpentinized ultramafic rocks are listed in Tables 3 and 4. In general, chromian spinels from dunites and chromitite pods in Bir Tuluha ophiolite are closely similar with high-Cr variety and exhibit narrow compositional variations, while they are intermediate-Cr variety in the host harzburgites. Chromian spinels in harzburgite host show intermediate composition, having lower Cr_2O_3 contents (40.1–45.9 wt%, 43.7 wt% on average) compared with those in dunite envelopes and chromitite pods. The Cr-ratio of harzburgite chromian spinels display values varying from 0.49 to 0.57, with an average of 0.54 (Table 3). Chromian spinels in dunite show restricted compositional ranges; the Cr_2O_3 content varies from 53.0 to 57.8 wt% (55.9 wt% on average). The Cr-ratio of dunite chromian spinels is remarkably high varies from 0.73 to 0.78 (0.76 on average) (Table 3). On the other hand, chromian spinels of all chromitite pods are of high-Cr varieties; having high Cr_2O_3 content 56.9 up to 62.1 wt%, with an average of 60.0 wt% (Table 4). The Cr-ratio of chromitite chromian spinels, like those in the dunite envelopes, is remarkably higher than those in the harzburgite host. It varies from 0.72 to 0.81, with an average of 0.76 (Table 4). The TiO_2 content of chromian spinel in all rock varieties (harzburgites, dunites and chromitites) are very low <0.25 wt %, which is a characteristic feature of ophiolitic upper mantle complexes.

The Mg-ratio (=Mg/(Mg + Fe^{+2}) atomic ratio) of chromian spinels in harzburgites, dunites and chromitites show narrow compositional variations, have a range of 0.56–67, 0.51–0.54, and 0.68–0.74, respectively (Tables 3 and 4), but is variable and inversely correlated with Cr-ratio. The Fe^{3+}-ratio (=Fe^{3+}/(Fe^{3+}+Cr + Al) atomic ratio) of chromian spinel is very low in all rock varieties (<0.07) (Tables 3 and 4). The very low Fe^{3+}-ratio, on one hand, and intermediate to high Cr-ratio and Mg-ratio, on the other hand, of

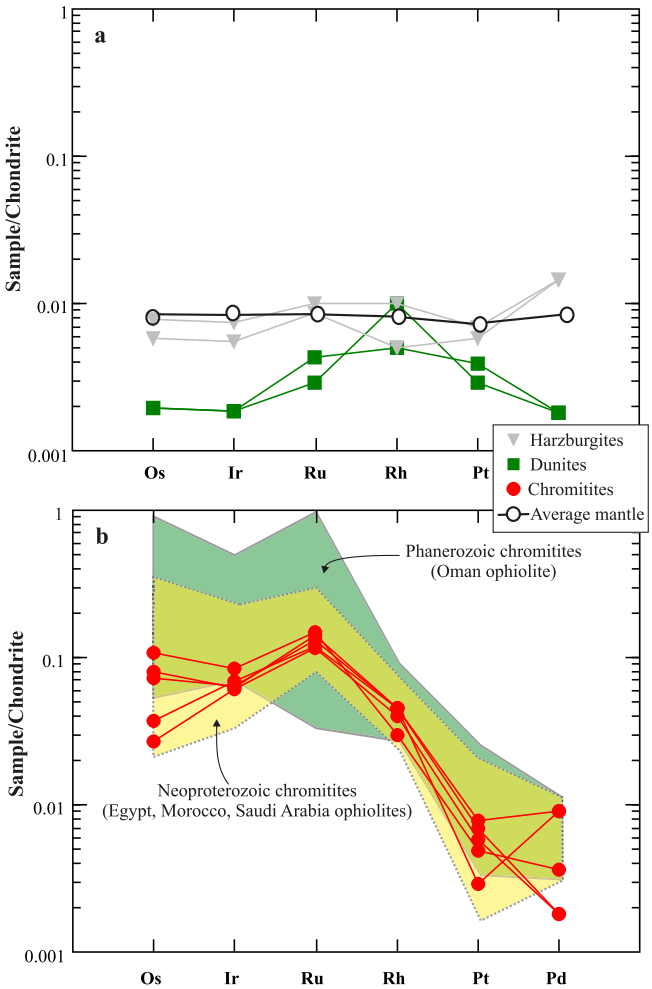

Fig. 5. Chondrite normalized PGE patterns from Bir Tuluha ophiolite. (a) serpentinized dunites and harzburgites, and (b) podiform chromitites. The average mantle PGE patterns and compositional fields of other ophiolite complexes are shown in (a) and (b), respectively, for comparison. Normalizing values currently in use are taken from Naldrett and Duke (1980; cf. 514, 540, 690, 200, 1020 and 545 for Os, Ir, Ru, Rh, Pt and Pd, respectively).

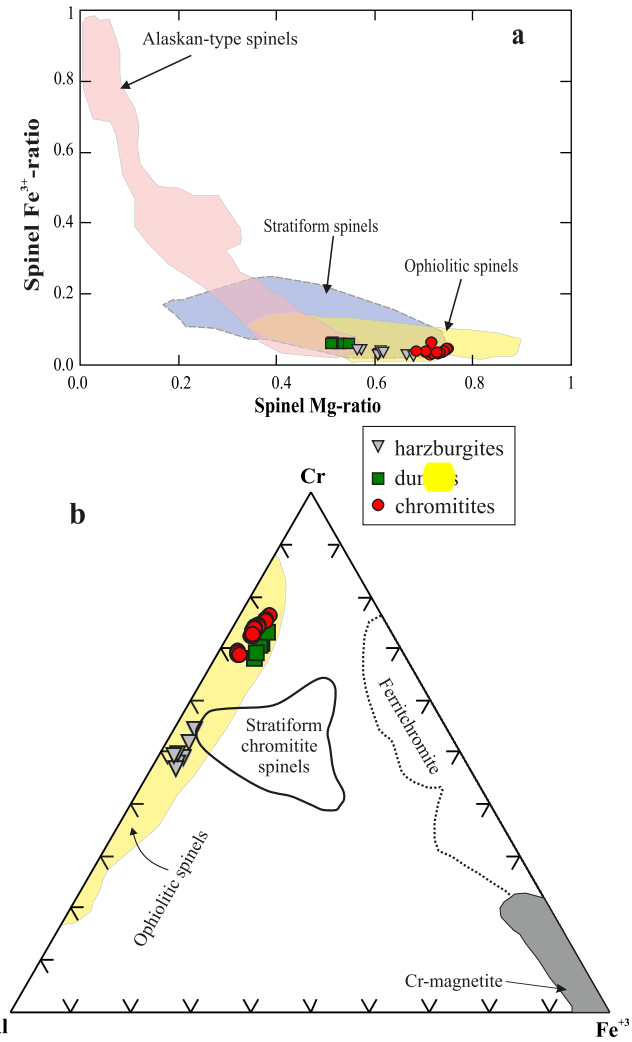

Fig. 6. (a) Fe^{3+}-ratio ($Fe^{3+}/(Fe^{3+} + Al + Cr)$ atomic ratio) versus Mg-ratio ($Mg/(Mg + Fe^{2+})$ atomic ratio) variation diagram, and (b) Cr-Al-Fe^{3+} triangle diagram of spinels from Bir Tuluha ophiolite. Discriminating fields of ophiolite, stratiform and Alaskan-type complexes (Irvine, 1967; Barnes and Röeder, 2001; Helmy and El Mahallawi, 2003; Ahmed et al., 2008) are presented for comparison.

chromian spinels in the Bir Tuluha upper mantle rocks are almost similar to chromian spinels from ophiolitic complexes elsewhere (Fig. 6a), which are clearly distinguished from the Alaskan-type and layered intrusion complexes (Barnes and Röeder, 2001; Farahat and Helmy, 2006; Ahmed et al., 2008; Helmy et al., 2014, 2015; Abdel Halim et al., 2016). This is also clearly shown in the Cr-Al-Fe^{3+} triangle diagram (Fig. 6b), where there is a continuous trend from intermediate- to high-Cr chromian spinels. The chromian spinels of ophiolitic complexes show progressive increase in Cr-ratio and decrease in Fe^{3+}-ratio (Fig. 6a, b).

5.2. Platinum-group minerals (PGM)

Platinum-group minerals (PGM) are described from chromitites of the Bir Tuluha area for the first time. Several PGM grains, up to 40 μm in size, were identified by reflected-light microscopy and quantitatively analyzed using electron microprobe microanalyzer. Totally, sixteen spot analyses in 11 PGM grains revealed Ru-rich laurite (RuS_2) as the only PGM phase encountered in the studied chromitite samples. Based on the PGE distribution patterns and mineralogy, the Bir Tuluha ophiolite belongs to the "unimodal" type, which is characterized by the predominance Ru-rich laurite and steep negative PGE slopes from Ru to Pt. Large PGM grains show more or less homogeneous chemical composition from core to rim, which are also mostly similar to those of smaller size grains (Table 5). The Os and Ir contents of the analyzed laurite grains vary from 0.42 to 5.86 wt% (2.59 wt% on average), and from 1.19 to 6.21 wt% (2.94 wt% on average), respectively (Table 5). The Os and Ir content of the analyzed laurite grains are very low compared with the normal Os-rich laurites from Proterozoic and Phanerozoic podiform chromitites (Ahmed and Arai, 2003; Ahmed, 2007). The Ru content of the analyzed laurite displays restricted range; it varies from 48.97 to 55.44 wt%, with an average of 52.88 wt%. The Ru ratio (Ru/(Ru + Os + Ir)) varies from 0.86 to 0.95, with an average of 0.91, which indicates an Os-poor laurite variety (Table 5). The Pt, Rh and Pd contents are also detectable (Table 5).

6. Discussion

6.1. Primary composition and the effect of serpentinization

Bulk-rock composition of ultramafic rocks and their mineral constituents can be easily modified, to variable extents, by low-temperature hydrothermal alteration (i.e., serpentinization) and metamorphism. The dunites and harzburgites of Bir Tuluha

ophiolite show no evidence of metamorphism; they consistently show high contents of MgO and low contents of CaO and SiO_2 (Table 1), indicating negligible effect of serpentinization on the distribution of major elements. The serpentinized dunites and harzburgites also have uniform and narrow range of MgO/SiO_2 ratios (<1), which indicates that Mg^{2+} and Si^{4+} remain immobile during serpentinization (Iyer et al., 2008). Furthermore, the very low sum of total REE (mostly below the detection limits) in the serpentinized dunites and harzburgites is another evidence that serpentinization has a negligible effect on the major and minor elements of the ultramafic protolith (Polat et al., 2007; Ordóñez-Calderón et al., 2008). In addition, the chondrite normalized PGE patterns of the chromitites and associated ultramafic rocks do not show any irregular jagged features that characterize a post-magmatic remobilization.

Mineralogically, the primary silicate minerals of dunite and harzburgite are completely altered to secondary ones; chromian spinel is so far the only primary mineral that survived alteration, reflecting the primary characteristics of ultramafic protolith. The alteration process is represented mainly by low-temperature serpentinization that produces serpentine minerals after olivine and pyroxenes. Ferritchromite and Cr-rich magnetite along the peripheries and cracks of chromian spinel grains are other alteration products in dunites and harzburgites, and to a lesser extent, in chromitites. There are several lines of evidence from mineral chemistry that can attest the primary magmatic composition of the studied chromian spinels in the upper mantle rocks, such as: (1) narrow range of chromian spinel composition in chromitite deposits and associated peridotites, (2) limited distribution, or even absence of ferritchromite alteration products of chromian spinel, (3) very low TiO_2 contents of chromian spinels in all rock varieties that testifies the primary residual nature.

Accordingly, the whole-rock compositions and mineral chemistry of the studied serpentinized dunites, harzburgites and chromitites are interpreted to represent the primary ultramafic rocks, with minor effect of serpentinization on the primary composition. The obtained analytical results in the present study can thus be safely used to estimate the parental melt composition and constrain the tectonic settings under which the Bir Tuluha ophiolite was formed.

6.2. Parental melt composition

Although dunite envelopes and harzburgite host are completely serpentinized, chromian spinels in these rocks and their associated massive chromitites are less affected by post magmatic alteration; ferritchromit and Cr-rich magnetite are restricted only along fractures and as very thin rims around chromian spinel grains. The intact primary chromian spinel cores which display limited or no compositional changes are used to calculate the parental melt composition. The parental melt composition involved in the formation of Bir Tuluha ultramafic rocks is represented here by the Al_2O_3, TiO_2 contents (wt%) and FeO/MgO ratio. The Al_2O_3 content of the parental melt is calculated using the equation of Maurel and Maurel (1982) for spinel-liquid equilibrium at 1 bar, where $(Al_2O_3)_{spinel} = 0.035(Al_2O_3)^{2.42}_{liquid}$. The FeO/MgO ratio of the parental melt is also calculated using the equation of Maurel and Maurel (1982) $\ln(Feo/MgO)_{spinel} = 0.47–1.07Y^{Al}_{spinel} + 0.64Y^{Fe+3}_{spinel} + \ln(FeO/MgO)$, where, $Y^{Al}_{spinel} = Al/(Cr + Al + Fe^{+3})$ and $Y^{Fe+3}_{spinel} = Fe^{+3}/(Cr + Al + Fe^{+3})$. The TiO_2 content of the parental melt is calculated using the equation of Rollinson (2008) for spinel-liquid equilibrium, given as $TiO_{2(melt)} = 1.0963 \times TiO_2\,{}^{(7863)}_{spinel}$.

The calculated Al_2O_3 and TiO_2 values and FeO/MgO ratios of the parental melt are given in Table 6, which is also compared with different melt compositions from various tectonic settings, such as: Oman ophiolite (Rollinson, 2008), Eastern Desert Proterozoic ophiolite, Egypt (Ahmed, 2013), Neoproterozoic ophiolite of Northwestern Saudi Arabia (Ahmed et al., 2012; Ahmed and Habtoor, 2015), Archean Nuasahi and Sukinda layered complexes (Mondal et al., 2006), average back-arc basin basalt (BABB) magma (Pearce et al., 2000; Kamenetsky et al., 2001), average worldwide boninites and mid-ocean ridge basalt (MORB) magmas (Wilson, 1989). The melt composition in equilibrium with Bir Tuluha chromitites and associated dunite envelopes is mostly similar to an arc environment (Table 6 and Fig. 7a). The Al_2O_3, TiO_2 contents and the FeO/MgO ratio of the parental melt in chromitites range from 10.21 to 12.29 wt%, 0.17 to 0.28 wt%, and 0.61 to 0.79, respectively (Table 6). The melt composition estimated from the dunite chromian spinels is comparable to that chromitite pods having the ranges of 10.67–11.56 wt% for Al_2O_3, 0.33–0.36 wt% for TiO_2, and 1.40–1.67 for FeO/MgO ratio (Table 6). On the other hand, the melt composition in equilibrium with the host harzburgite shows remarkably different values of Al_2O_3 (14.66–15.85 wt%), TiO_2 (0–0.13 wt%) and FeO/MgO (0.99–1.62 wt%) (Table 6). The similarity in chromian spinel chemistry in chromitites and surrounding dunite envelopes, and their estimated parental melt composition are most probably due to their formation by a similar common magmatic process, namely melt-rock interaction, which will be explained later in this article. However, the difference in chromian spinel chemistry and parental melt composition in

Table 6
Estimated minimum, maximum and (average) values of Al_2O_3, FeO/MgO and TiO_2 of parental melts in Bir Tuluha ophiolite, in comparison with primitive melts of different tectonic settings.

	$Al_2O_{3(melt)}$	$TiO_{2(melt)}$	FeO/MgO (melt)	References
Serpentinized dunites	10.67–11.56 (11.12)	0.33–0.36 (0.35)	1.40–1.67 (1.54)	This study
Serpentinized harzburgites	14.66–15.85 (15.26)	0–0.13 (0.07)	0.99–1.62 (1.31)	This study
Chromitites	10.21–12.29 (11.25)	0.17–0.28 (0.23)	0.61–0.79 (0.70)	This study
Dunites	10.52–11.71	0.00–0.04		Ahmed and Habtoor (2015)
Peridotites	10.36–11.33	0.00–0.03		
Chromitites	8.51–9.02	0.00–0.06		
Dunites	13.89–15.11		1.28–1.97	Ahmed et al. (2012)
Peridotites	14.55–16.41		1.12–1.84	
Chromitites	10.18–13.95	0.23–0.55	0.72–1.17	
Boninites (SSZ)	10.60–14.40	0.10–0.52	0.70–1.40	Wilson (1989)
MORB	~15	0.32–2.20	1.20–1.60	Wilson (1989)
BABB	~17	0.45–1.45		Kamenetsky et al. (2001), Pearce et al. (2000)
Deep chromitites (Oman)	11.8–12.9	0.23–0.34		Rollinson (2008)
Egypt SED	9.12–12.12		0.42–0.79	Ahmed et al. (2013)
Stratiform chromitite	11.5		0.74	Mondal et al. (2006)

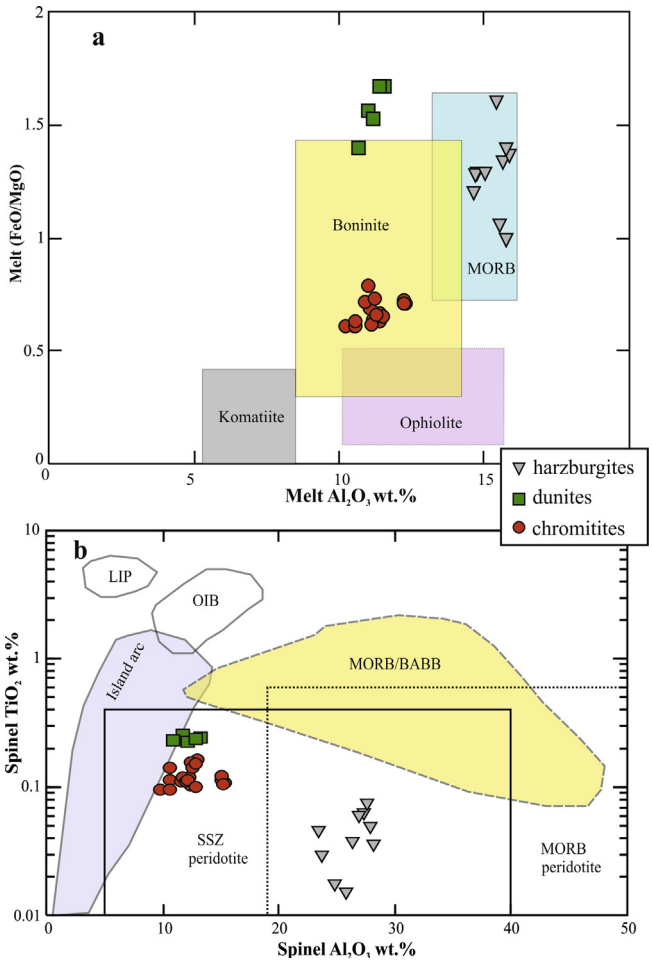

Fig. 7. (a) Estimated variation of the parental melt composition in terms of FeO/MgO versus Al_2O_3 wt% in the Bir Tuluha ophiolite. Tectonic compositional fields are from Barnes and Röeder (2001). (b) Plot of TiO_2 versus Al_2O_3 wt% in chromian spinels. Tectonic discrimination fields are after Kamenetsky et al. (2001). SSZ: Supra-subduction zone; LIP: large igneous province; MORB: mid-ocean ridge basalt; OIB: ocean island basalt.

harzburgite host, on one hand, and those in the associated dunites and chromitites, on the other hand, is mostly due to the difference in the process of formation and tectonic setting.

In comparison with the melts from different tectonic settings (Wilson, 1989; Kamenetsky et al., 2001; Falloon et al., 2008), the calculated parental magma composition of Bir Tuluha podiform chromitites and associated dunite envelopes shows fair consistency with a boninitic magma composition ($Al_2O_{3(boninite)}$ = 10.6–14.4 wt %, $FeO/MgO_{(boninite)}$ = 0.7–1.14; Wilson, 1989) (Fig. 7a) produced in a supra-subduction zone (SSZ) environment. This is in harmony with the strong affinity between ophiolites and boninites in terms of their chromian spinel composition, where boninite is widely considered as the dominant parental magma for podiform chromitite deposits in ophiolites (Barnes and Röeder, 2001). On the other hand, the estimated melt composition in equilibrium with the host harzburgite shows less depleted character than chromitites and dunite envelopes, which is fairly consistent with the composition of MORB magmas ($Al_2O_{3(MORB)}$ = ~15 wt%, $FeO/MgO_{(MORB)}$ = 1.2–1.6; Kamenetsky et al., 2001) (Fig. 7a). Similar diversity in melt compositions with boninitic and MORB affinities have also been suggested to be the source of high-Cr and high-Al chromitites, respectively, together with the peridotites from other complexes worldwide (Melcher et al., 1997; Mondal et al., 2006; Rollinson, 2008; González-Jiménez et al., 2011; Ahmed et al., 2012; Ahmed, 2013; Ahmed and Habtoor, 2015).

6.3. Petrogenesis and tectonic implications

6.3.1. Chromian spinel implications

The chemical composition of chromian spinel can be used as a powerful petrogenetic indicator on magma genesis and different tectonic settings (Dick and Bullen, 1984; Arai, 1994; Roeder, 1994; Barnes and Röeder, 2001; Kamenetsky et al., 2001; Arai et al., 2011). Chromian spinel with different chemical compositions reflects a formation in different tectonic settings (arc-forearc, BAB and MOR) (Dick and Bullen, 1984; Arai, 1994; Arai and Yurimoto, 1994; Roeder, 1994; Barnes and Röeder, 2001). Falloon and Danyushevsky (2000) suggested that the association of boninitic, high-Mg andesite and arc tholeiite magmas and Cr-rich podiform chromitites in highly refractory peridotite reflects high temperature, low pressure and high P_{H2O} conditions, and concluded that boninites are found exclusively in arc-forearc terrains.

All the collected chromitite pods and their dunite envelopes throughout the entire area of Bir Tuluha display homogeneous geochemical characteristics, having high-Cr variety. The collected samples from the harzburgite host throughout the whole area are also homogeneous with intermediate-Cr variety. Thus, based on the geochemical characteristics of chromian spinel, two groups of data can be recognized: (1) chromian spinel from chromitite pods and associated dunite envelopes, and (2) chromian spinel from harzburgite host. The average Cr-ratio in chromian spinel of chromitite pods and dunite envelopes is 0.76 (0.72–0.81, and 0.73–0.78, respectively). The average Cr-ratio of chromian spinel in harzburgite host is distinguishable from the earlier ones; it is 0.54 (0.49–0.57) (Tables 3 and 4). Harzburgite, which is the main mantle lithology in the Tuluha ophiolite, with intermediate refractory nature, is the most common host for podiform chromitites in ophiolites of different tectonic settings and ages (Arai, 1997), and it is the most common lithology in the ophiolitic mantle section worldwide (Ahmed and Arai, 2002; Le Mee et al., 2004). This is consistent with the abundance of medium- to large-scale chromitite pods within harzburgite in the study area, as well as other areas in the Arabian Shield of Saudi Arabia (Ahmed et al., 2012; Ahmed and Habtoor, 2015). The intermediate average Cr-ratio of chromian spinels and the low PGE contents with approximately unfractionated patterns (Fig. 6a) of the studied harzburgite host, suggest a mantle residue after a low degree of partial melting at MOR setting. It is highly possible, therefore, that the harzburgite host of Bir Tuluha ophiolite was derived from the ophiolitic upper mantle section produced at a MOR environment. This is strongly supported by the estimation of parental melt composition in equilibrium with mantle harzburgite, in terms of its Al_2O_3 contents and FeO/MgO ratios, where all the calculated data of harzburgite chromian spinels are entirely plotted within the MOR field (Fig. 7a). Furthermore, in the Al_2O_3–TiO_2 binary diagram (Fig. 7b), all the analyzed chromian spinels from harzburgite are also entirely plotted within the MOR peridotite field.

Although, in most cases, the mantle harzburgite is rather homogeneous in petrological characteristics, several ophiolite localities in the world show diversity in chromitite types, with two different compositions (high-Al and high-Cr varieties). Among those are, for example Northern Oman ophiolite (Ahmed and Arai, 2002), Rayat ophiolite Iraq (Ismail et al., 2009), Wadi Al Hwanet and Al'Ays ophiolites Saudi Arabia (Ahmed et al., 2012; Ahmed and Habtoor, 2015). In such cases, at least two contrasting evolutionary stages have been ascribed in response to a switch of tectonic setting: the high-Al chromitite with Cr-ratio of chromian spinel <0.6 was formed from a melt of MOR/BAB affinity, and the high-Cr chromitite with Cr-ratio of chromian spinel >0.6 was in equilibrium with the melt of boninitic affinity (Ahmed and Arai, 2002; Ahmed and Habtoor, 2015). Thus, chromitite deposits with high Cr-ratio of chromian spinel are most probably produced by the interaction

between high degree partial melts with mantle peridotite, possibly in a supra-subduction zone environment. In the present study, throughout the whole area of Bir Tuluha ophiolite belt, all the studied chromitite pods are uniform in their chemical composition, including Cr-ratio of chromian spinel higher than 0.7. The high Cr-ratio of chromian spinel strongly implies that these chromitite deposits were formed either from a high-degree partial melt or from the melting of already depleted peridotite. This kind of second-stage magma is most easily formed in the supra-subduction zone environment, where H_2O is supplied as a flux from the subducted slab. This interpretation is strongly supported by the estimation of parental melt composition in equilibrium with podiform chromitites, where the Bir Tuluha chromitite pods are entirely plotted within the boninite field (Fig. 7a). In addition, chromian spinel of chromitite pods is also plotted within the SSZ field of the Al_2O_3–TiO_2 discrimination diagram (Fig. 7b). The Bir Tuluha chromitites are composed of a highly refractory chromian spinel with high Cr-ratio, Mg-ratio (0.68.0–0.75), and very low TiO_2 content (0.09–0.15 wt%), which is consistent with a boninitic parentage, where all the chromitite samples fall within the boninite field (Fig. 8a, b). The relative enrichment of Bir Tuluha bulk rock samples in the fluid-mobile elements (Rb and Ba) and strong depletion in the compatible non-fluide mobile elements (Sr, Nb, Ta, Hf, Zr and REE) is another evidence for the formation in a SSZ environment.

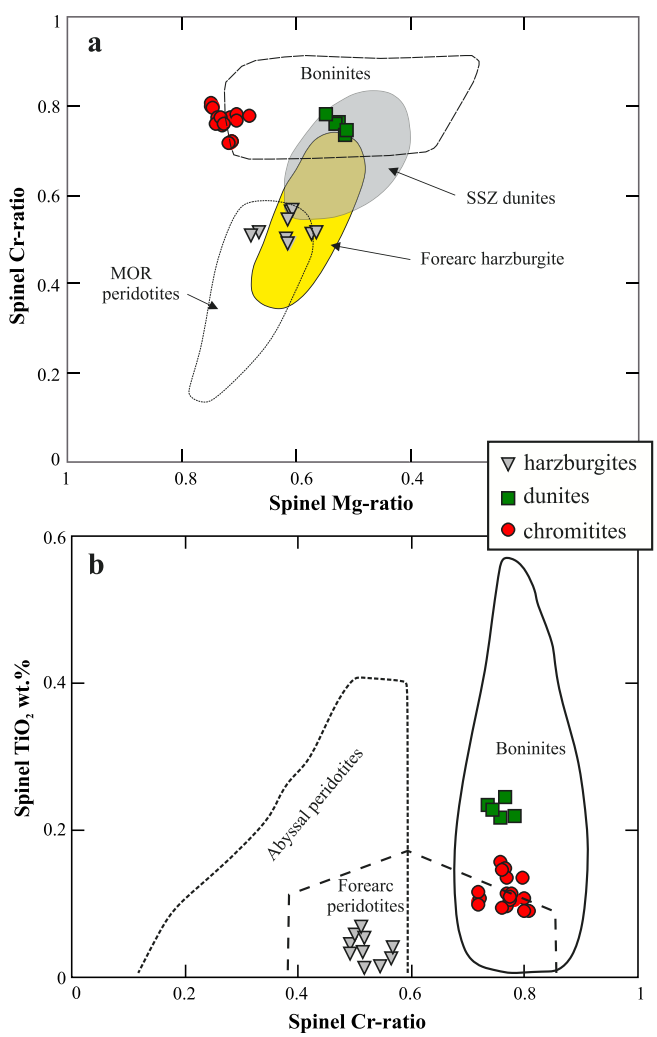

Fig. 8. (a) Cr-ratio (Cr/(Cr + Al) atomic ratio) versus Mg-ratio (Mg/(Mg + Fe^{2+}) atomic ratio) diagram for chromian spinels of the Bir Tuluha ophiolitic rocks. Tectonic fields of forearc harzburgites/peridotites and SSZ dunites are from Ishii et al. (1992), Parkinson and Pearce (1998), Pearce et al. (2000), the abyssal peridotites field is from Dick and Bullen (1984), and the boninites field is from van der Laan et al. (1992).

The melt-rock reaction process and a subsequent melt mixing model is the most recent acceptable process for the formation of podiform chromitite (Zhou et al., 1996; Arai and Yurimoto, 1994; Arai, 1997; Zhou and Robinson, 1997). The melt-rock reaction model is strongly supported by the wide occurrence of dunite envelopes around most podiform chromitites within the mantle harzburgite host. In this model, as a result of melt interaction with wall peridotites, clinopyroxene and orthopyroxene are chiefly dissolved while olivine is precipitated, this produces the dunite envelopes. The resultant melt becomes rich in Si and Cr, which subsequently mixes with new batches of boninitic melts from which the chromitite pods and associated dunite envelopes are formed (Arai and Yurimoto, 1994; Zhou et al., 1996). This process gives a zonal pattern grading outward from the chromitite pods to the harzburgite host, passing through the dunite envelopes (Zhou et al., 1996; Arai, 1997; González-Jiménez et al., 2011). In most cases, the chromian spinel of podiform chromitites and their associated dunite envelopes are similar in composition, confirming their genetic relationship via melt-peridotite interaction (Zhou et al., 1996; Ahmed et al., 2001; Ahmed and Arai, 2002; González-Jiménez et al., 2011). In few cases, however, the chromian spinel composition in dunite envelopes is in between those in the podiform chromitites and harzburgite host (Ahmed et al., 2012). This is most probably based on the melt-rock ratio contributed to the chromitite–dunite formation. The higher the melt-rock ratio, the thicker the resultant dunite envelopes, while the lower the melt-rock ratio, the thinner the resultant dunite envelopes (Ahmed et al., 2012). In the earlier case where the melt-rock ratio is relatively high, chromian spinel composition of chromitite-dunite pairs will be more or less similar, while in the latter case where melt-rock ratio is low, chromian spinel composition will be intermediate between those in the chromitites and the harzburgite host (Ahmed et al., 2012). In the present study, all the chromitite pods have thin dunite envelopes (0.5–2 m in thickness) with a zonal pattern grading outward into harzburgite host, suggesting a formation by interaction between melt and residual mantle harzburgite. The widely distributed medium- to large sized podiform chromitite deposits and their surrounding thin dunite envelopes in Bir Tuluha ophiolite belt, along with their high-Cr variety, imply the pervasive invasion of boninitic melt within MOR peridotite host.

It is noteworthy that large-scale ophiolitic chromitite pods hosted by moderately refractory peridotite with intermediate Cr-ratio of chromian spinel (Arai, 1994, 1997), is thought to have been formed by the interaction between boninitic melt and variably refractory peridotite (Zhou et al., 1998).

6.3.2. PGE and PGM implications

The platinum-group elements (PGE) and platinum-group minerals (PGM) can be used as a potential geochemical monitor for the deep-seated processes taking place in the mantle. Due to the siderophile and chalcophile nature of these precious metals, they give constraints on the degree of partial melting and sulfur saturation of a melt produced in the upper mantle; they tend to be strongly fractionated into a sulfide phase (Arculus and Delano, 1981; Naldrett, 1981; Garuti et al., 1997). In general, podiform chromitites show variable PGE contents, usually less than 500 ppb, and Pd_N/Ir_N ratios between 0.8 and 0.1, although in some instances they may contain higher total PGE (>750 ppb) and display very low Pd_N/Ir_N ratios (<0.1) (Page and Talkington, 1984; Leblanc, 1991; Zhou et al., 1998; Ahmed and Arai, 2002; Büchl et al., 2004; Gervilla et al., 2005). They are characterized by IPGE

enrichment and depletion in PPGE, resulting in a general negative slope in PGE diagrams. Due to the low mobility of Cr and PGE beneath the MOR setting, they generally behave compatibly during dry partial melting in the upper mantle (Mitchell and Keays, 1981; Dick and Bullen, 1984; Büchl et al., 2004). In contrast to that, PGE, especially PPGE, behave incompatibly during hydrous partial melting in a SSZ setting, where the degree of partial melting is much higher than in a MOR setting. This leaves behind a podiform chromitite that is highly depleted in PPGE and notably enriched in Cr and IPGE (Zhou et al., 1998; Ahmed and Arai, 2002; Büchl et al., 2004).

The Bir Tuluha chromitite pods contain up to 217 ppb total PGE, which are highly enriched in IPGE and strongly depleted in PPGE, forming a steep negative slope in the PGE spider diagrams with very low PPGE/IPGE ratios (average Pd_N/Ir_N ratio of 0.08), similar to most of the ophiolitic chromitites worldwide (Page and Talkington, 1984; Leblanc, 1991; Zhou et al., 1998). The main hosts of PPGE, i.e., Pd and Pt, in the upper mantle rocks are the base metal sulfides (Mitchell and Keays, 1981; Luguet et al., 2003). High degrees of partial melting could lead to complete dissolution of the sulfides in the mantle source being melted; the Pd and Pt would be removed from produced melt (Zhou et al., 1998), leaving behind a mantle residue highly depleted in these elements. The distinctive decoupling of the two PGE subgroups, along with the high Cr-ratio of chromian spinels (> 0.70), strongly implies that a second-stage melting was involved in the formation of the Bir Tuluha chromitites. This also implies that the chromitite forming magma was originally highly S-undersaturated (e.g., boninitic magma) to be able to dissolve the mantle sulfides and partly remove the Pd and Pt resident in their mantle host rocks. Thus, the interaction between boninitic melts and wall peridotite would have contributed to the formation of PPGE-depleted podiform chromitites in Bir Tuluha upper mantle. This is most easily formed by hydrous melting at a SSZ setting, where the down-going slab is the source of water which, in turn, promotes the removal of PGE from their mantle source (Matveev and Ballhaus, 2002; Büchl et al., 2004).

There is now a general consensus that the PGM inclusions represent magmatic minerals entrapped by the growing chromian spinel crystals (Stockman and Hlava, 1984; Augé, 1988; Ferrario and Garuti, 1990; Torres-Ruiz et al., 1996) rather than the products of subsolidus exsolution from the host chromian spinel. The perfect polygonal euhedral shape of the laurite crystals and their sporadic distribution within fresh chromian spinel strongly suggest that laurite grains in the Bir Tuluha chromitites represent a high-temperature phase on the liquidus of a primitive magma. Experimental studies (Brenan and Andrews, 2001) suggest that Ru, Os and Ir tend to be retained in alloys and, to a lesser extent, sulfides, at a relatively low sulfur fugacity (fS_2) and high temperature (1200–1300 °C) conditions. Under such conditions, laurite shows a composition of nearly pure RuS_2 with low concentrations of Os and Ir (Brenan and Andrews, 2001). Thus, the formation of Os-rich laurite and erlichmanite (OsS_2) requires a higher fS_2 than for Ru-rich laurite. Consequently, the Ru substitution by Os in laurite is promoted by an increase of fS_2 (Stockman and Hlava, 1984; Woods, 1987; Brenan and Andrews, 2001). Hence, the common abundance of Os-poor (= Ru-rich) laurite and the absence of any other Os–Ir sulfides and/or alloys in Bir Tuluha chromitites suggest that the initial fS_2 of the magma was too low for the formation of Os-rich laurite. It is highly possible, therefore, that the magma involved in the formation of Bir Tuluha chromitites was S-undersaturated, and that the Os-poor laurite crystallized at a lower fS_2 than in other complexes, where the laurite composition is more Os-rich (Ahmed and Arai, 2003; Ahmed, 2007). High temperature boninitic melt with low fS_2 is thus, the most suitable candidate for the formation of Bir Tuluha chromitites.

6.4. Bir Tuluha ophiolite among others: A comparison

From the literature review, ophiolite complexes and their podiform chromitites can be categorized under three main periods in the Earth's history: (1) Archean (3800–2500 Ma), (2) Proterozoic (early and late: 2500–542 Ma), and (3) Phanerozoic (<542 Ma). The Archean and the early Proterozoic ophiolites together with their podiform chromitites, show narrow distribution in the Earth's geologic record compared with the late Proterozoic and Phanerozoic ones. The chromitite dimensions were extremely small in the Archean and early Proterozoic age, while they became larger and abundant in the late Proterozoic and Phanerozoic ones (unpublished compiled data of the authors). The available data on chromitites and their host peridotites of the Archean mantle (Kusky et al., 2004; Huang et al., 2004) shows highly refractory composition; the Cr-ratio of chromian spinels in chromitites is very restricted and varies from 0.7 to 0.9. The Cr-ratio of chromian spinel in the host harzburgite is also high, around 0.7 (Fig. 9). The few available petrological data of chromitites and associated peridotites from the early Proterozoic ophiolites (Liipo et al., 1995; Vuollo et al., 1995; Peltonen et al., 1998; Peltonen and Kontinen, 2004), are rather extraordinary, where the Cr-ratio of chromitite

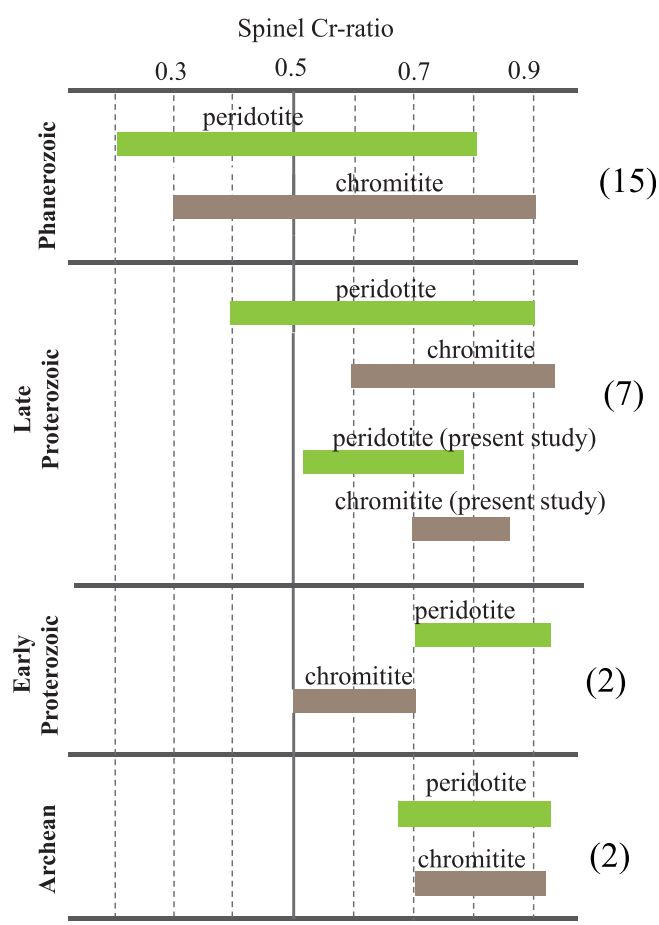

Fig. 9. Compositional ranges of chromian spinel Cr-ratio in the upper mantle rocks (peridotites and chromitites) from different ophiolite suites of different ages compared with the Bir Tuluha ophiolite. Note the more restricted and high Cr-ratio of chromian spinels in the Archean and Proterozoic ophiolites compared with those of Phanerozoic ones. Numbers between brackets refer to the number of ophiolitic complexes examined. Source data for the Phanerozic ophiolites is from Arai (1997). For the Late Proterozoic ophiolites (Pan-African ophiolites) see Ahmed et al. (2012), Ahmed (2013), Khedr and Arai (2013), Ahmed and Habtoor (2015). For the Early Proterozoic ophiolites see Liipo et al. (1995), Vuollo et al. (1995), and for the Archean ophiolites see Li et al. (2002), Huang et al. (2004), Kusky et al. (2004).

chromian spinel (~0.6) is fairly lower than those of the host peridotites (0.8–0.9) (Fig. 9).

Ophiolites become more common in the late Proterozoic age in several places worldwide, almost all of them are found to contain podiform chromitites. Late Proterozoic ophiolites are abundant in Africa and Western Arabia; among these, the Arabian-Nubian Shield which is very famous with numerous ophiolite complexes, mostly contain high-Cr chromitites (Ahmed et al., 2001, 2005, 2012; Ahmed and Habtoor, 2015). Al-rich chromitite varieties started to appear in the late Proterozoic ophiolites, although the majority is Cr-rich (Fig. 9) with boninitic affinity. The Bir Tuluha ophiolite is one of the late Proterozoic ophiolite complexes in the Arabian-Nubian Shield, where numerous podiform chromitites are widely distributed.

Ophiolite complexes are very popular in almost all orogenic belts during the Phanerozoic eon (Moores, 1982; Moores et al., 2000; Beccaluva et al., 2002, 2004). Podiform chromitites are very common and large in size in the Tethyan ophiolites of the late Paleozoic to Mesozoic age. Their host mantle peridotites have a wide range of chromian spinel composition; Cr-ratio varies from 0.2 to 0.8 (Fig. 9), with an intermediate average Cr-ratio, around 0.5, serving as the most common host for large podiform chromitites in the Phanerozoic ophiolites. With few exceptions, all known Phanerozoic ophiolites possess less refractory peridotites and chromitites than the Precambrian ophiolites (Fig. 9). Diversity in chromian spinel chemistry and PGE contents in podiform chromitites become more distinct in the Phanerozoic ophiolites (Ahmed and Arai, 2002).

The Bir Tuluha chromitite-dunite-harzburgite association is very similar to that in the late Proterozoic ophiolite complexes, especially those in the Arabian-Nubian Shield. The chromian spinel chemistry of podiform chromitites and associated dunite envelopes are very similar, including high Cr-ratio (>0.7), which are most probably formed by the interaction between boninitic melt and wall rock peridotites in an arc setting. The common host of these high-Cr chromitites is the mantle harzburgite with intermediate Cr-ratio of chromian spinel. The main difference of Bir Tuluha ophiolite from the late Proterozoic ophiolite complexes is the absence of Al-rich chromitites which are quite common in many Proterozoic and Phanerozoic ophiolite complexes (Ahmed et al., 2001, 2012; Ahmed and Arai, 2002; Miura et al., 2012). Based on the PGE distribution patterns and mineralogy, the Bir Tuluha ophiolite belongs to the "unimodal" type which is characterized by the predominance Ru-sulfide mineralogy and negatively steep PGE slopes from Ru to Pt. Laurite is, by far, the sole primary PGM found in all chromitite pods of Bir Tuluha ophiolite. This is, in most cases, different from other ophiolite complexes of Proterozoic and Phanerozoic ages where both "unimodal" and "bimodal" types are common (Ahmed and Arai, 2003, and references therein).

7. Conclusions

The mantle section of the Bir Tuluha ophiolite is dominated by severely serpentinized harzburgites with less abundant dunites and medium- to large-scale chromitite pods. Composition of chromian spinels in chromitites and dunite envelopes displays little variation, which is quite different from those in the harzburgite host. The high Cr-ratio of chromian spinels in chromitites and associated dunite envelopes along with low TiO_2 content, suggests their formation by the interaction between MOR mantle harzburgite with arc-related magma. This second stage melting could have a genetic linkage with boninite or high Mg arc tholeiitic melt produced by high degrees of partial melting above supra-subduction zone environment. The PGE distribution patterns for all chromitite pods display steep negative slopes from Ru to Pt, with clear decoupling of IPGE and PPGE, which support formation from a high degree partial melt of boninitic affinity. The common abundance of Ru-rich laurite as the sole primary PGM in chromitite pods suggest a low fS_2 and high temperature boninitic melt involved in the formation of Bir Tuluha chromitites. The estimated parental melt composition in equilibrium with the formation of podiform chromitites and associated dunite envelopes also indicates a boninitic parentage above a supra-subduction zone setting. Thus, the homogeneous high-Cr composition of chromian spinel in podiform chromitites and surrounding dunite envelopes within intermediate refractory mantle peridotite in Bir Tuluha ophiolite belt, suggests a pervasive interaction of boninitic melt with a MOR-type mantle peridotite. This situation is common in the late Proterozoic ophiolites, which show both the high-Cr and high-Al chromitite varieties hosted by intermediate refractory mantle peridotites. The Bir Tuluha ophiolite is relatively different from the Proterozoic and Phanerozoic ophiolites by the only presence of high-Cr chromitites and unimodal PGE/PGM type. The upper mantle of Bir Tuluha ophiolite has most probably been modified by a substantial amount of supra-subduction zone components after initially being formed in a MOR setting. This is materialized by the wide occurrence of homogeneous high-Cr podiform chromitites and their closely similar dunite envelopes.

Acknowledgements

This paper is a part from a PhD thesis of the first author who would like to express his gratitude to the staff members in the Department of Mineral Resources and Rocks of the Faculty of Earth Sciences, King Abdulaziz University, for their help and fruitful discussions during his research. The authors would like to thank two anonymous reviewers for their critical review and comments that greatly improved the earlier version of the manuscript. The guest editors, Sisir Mondal and Ria Mukherjee, are also thanked for their comments and handling the manuscript.

References

Abdel Halim, A.H., Helmy, H.M., Abd El-Rahman, Y.M., Shibata, T., El Mahallawi, M. M., Yoshikawa, M., Arai, S., 2016. Petrology of the Motaghairat mafic–ultramaficcomplex, Eastern Desert, Egypt: a high-Mg post-collisional extension-related layered intrusion. J. Asian Earth Sci. 116, 164–180.

Ahmed, A.H., 2007. Diversity of platinum-group minerals in podiform chromitites of the late Proterozoic ophiolite, Eastern Desert. Egypt: genetic implications. Ore Geol. Rev. 32, 1–19.

Ahmed, A.H., 2013. Highly depleted harzburgite–dunite–chromitite complexes from the Neoproterozoic ophiolite, south Eastern Desert. Egypt: a possible recycled upper mantle lithosphere. Precambr. Res. 233, 173–192.

Ahmed, A.H., Arai, S., 2002. Unexpectedly high-PGE chromitite from the deeper mantle section of the northern Oman ophiolite and its tectonic implications. Contrib. Mineral. Petrol. 143, 263–278.

Ahmed, A.H., Arai, S., 2003. Platinum-group minerals in podiform chromitites of the Oman ophiolite. Can. Miner. 41, 597–616.

Ahmed, A.H., Surour, A.A., 2016. Fluid-related modifications of Cr-spinel and olivine from ophiolitic peridotites by contact metamorphism of granitic intrusions in the Ablaharea, Saudi Arabia. J. Asian Earth Sci. 122, 58–79.

Ahmed, Z., Hariri, M.M., 2008. Neoproterozoic ophiolites as developed in Saudi Arabia and their oceanic and pericontinental domains. Arab. J. Sci. Eng. 33, 17–54.

Ahmed, A.H., Helmy, H.M., Arai, S., Yoshikawa, M., 2008. Magmatic unmixing in spinel from late Precambrian concentrically-zoned mafic-ultramafic intrusions, Eastern Desert, Saudi Arabia. Lithos 104, 85–98.

Ahmed, A.H., Arai, S., Attia, A.K., 2001. Petrological characteristics of podiform chromitites and associated peridotites of the Pan African ophiolite complexes of Egypt. Miner. Deposita 36, 72–84.

Ahmed, A.H., Arai, S., Yaser, M.A., Rahimi, A., 2005. Spinel composition as a petrogenetic indicator of the mantle section in the Neoproterozoic Bou Azzer ophiolite, Anti-Atlas, Morocco. Precambr. Res. 138, 225–234.

Ahmed, A.H., Arai, S., Abdel-Aziz, Y.M., Ikenne, M., Rahimi, A., 2009. Platinum-group elements distribution and spinel composition in podiform chromitites and associated rocks from the upper mantle section of the Neoproterozoic Bou Azzer ophiolite, Anti-Atlas, Morocco. J. Afr. Earth Sci. 55, 92–104.

Ahmed, A.H., Habtoor, A., 2015. Heterogeneously depleted Precambrian lithosphere deduced from mantle peridotites and associated chromitite deposits of Al'Ays ophiolite, Northwestern Arabian Shield, Saudi Arabia. Ore Geol. Rev. 67, 279–296.

Ahmed, A.H., Harbi, H.M., Habtoor, A.M., 2012. Compositional variations and tectonic settings of podiform chromitites and associated ultramafic rocks of the Neoproterozoic ophiolite at Wadi Al Hwanet, northwestern Saudi Arabia. J. Asian Earth Sci. 56, 118–134.

Al-Shanti, A.M., Gass, I.G., 1983. The upper Proterozoic ophiolite mélange zones of the easternmost Arabian shield. J. Geol. Soc. Lond. 140, 867–876.

Al-Shanti, A.M., El-Mahdy, O.R., 1988. Geological Studies and Assessment of Chromite Occurrences in Saudi Arabia: KACST Project No. AT-6-094.

Arai, S., 1994. Characterization of spinel peridotites by olivine-spinel compositional relationships: review and interpretation. Chem. Geol. 113, 191–204.

Arai, S., 1997. Control of wall-rock composition on the formation of podiform chromitites as a result of magma/peridotite interaction. Resour. Geol. 47, 177–187.

Arai, S., Yurimoto, H., 1994. Podiform chromitites of the Tari-Misaka ultramafic complex, Southwestern Japan, as mantle-melt interaction products. Econ. Geol. 89, 1279–1288.

Arai, S., Okamura, H., Kadoshima, K., Tanaka, C., Suzuki, S., Ishimaru, S., 2011. Chemical characteristics of chromian spinel in plutonic rocks: implications for deep magma processes and discrimination of tectonic setting. Island Arc 20, 125–137.

Arculus, R.J., Delano, J.W., 1981. Siderophile element abundances in the upper mantle: evidence for a sulfide signature and equilibrium with the core. Geochim. Cosmochim. Acta 55, 1159–1172.

Augé, T., 1988. Platinum-group minerals in the Tiebaghi and Vourinos ophiolitic complexes: genetic implications. Can. Miner. 26, 177–192.

Barnes, S.J., Röeder, P.L., 2001. The range of spinel compositions in terrestrial mafic and ultramafic rocks. J. Petrol. 42, 2279–2302.

Beccaluva, L., Coltorti, M., Di Girolamo, P., Melluso, L., Milani, L., Morra, V., Siena, F., 2002. Petrogenesis and evolution of Mt. Vulture alkaline volcanism (Southern Italy). Mineral. Petrol. 74, 277–297.

Beccaluva, L., Coltorti, M., Giunta, G., Siena, F., 2004. Tethyan vs. Cordilleran ophiolites: a reappraisal of distinctive tectono-magmatic features of supra-subduction complexes in relation to the subduction mode. Tectonophysics 393, 163–174.

Brenan, J.M., Andrews, D.R.A., 2001. High-temperature stability of laurite and Ru–Os–Ir alloys and their role in PGE fractionation in mafic magmas. Can. Miner. 39, 341–360.

Büchl, A., Brügmann, G., Batanova, V., 2004. Formation of podiform chromitite deposits: implications from PGE abundances and Os isotopic compositions of chromites from the Troodos complex, Cyprus. Chem. Geol. 208, 217–232.

Collenette, P., Grainger, D.J., 1994. Mineral resources of Saudi Arabia. Not including oil, natural gas and sulfur. DGMR Spec. Publ. SP-2, 55–68.

Dare, S.A.S., Pearce, J.A., McDonald, I., Styles, M.T., 2009. Tectonic discrimination of peridotites using fO_2–Cr and Ga–Ti–Fe^{3+} systematic in chrome-spinel. Chem. Geol. 261, 199–216.

Dick, H.J.B., Bullen, T., 1984. Chromian spinel as a petrogenetic indicator in abyssal and alpine type peridotites and spatially associated lavas. Contrib. Mineral. Petrol. 86, 54–76.

Falloon, T.J., Danyushevsky, L.V., 2000. Melting of refractory mantle at 1.5, 2, and 2.5 GPa under anhydrous and H_2O-undersaturated conditions: implications for the petrogenesis of high-Ca boninites and the influence of subduction components on mantle melting. J. Petrol. 41, 257–283.

Falloon, T.J., Green, D.H., Danyushevsky, L.V., McNeill, A.W., 2008. The composition of near-solidus partial melts of fertile peridotite at 1 and 1.5 GPa: implications for the petrogenesis of MORB. J. Petrol. 49, 591–613.

Farahat, E.S., Helmy, H.M., 2006. Abu Hamamid Neoproterozoic Alaskan-type complex, south Eastern Desert, Egypt. J. Afr. Earth Sci. 45, 187–197.

Ferrario, A., Garuti, G., 1990. Platinum-group mineral inclusions in chromitites of the Finero mafic-ultramafic complex (Ivrea-Zone, Italy). Mineral. Petrol. 41, 125–143.

Garuti, G., Fershtater, G., Bea, F., Montero, P., Pushkarev, E.V., Zaccarini, F., 1997. Platinumgroup elements as petrological indicators in mafic–ultramafic complexes of the central and southern Urals: preliminary results. Tectonophysics 276, 181–194.

Gervilla, F., Proenza, J.A., Frei, R., González-Jiménez, J.M., Garrido, C.J., Melgarejo, J.C., et al., 2005. Distribution of platinum-group elements and Os isotopes in chromite ores from Mayarí-Baracoa ophiolitic belt (eastern Cuba). Contrib. Mineral. Petrol. 150, 589–607.

González-Jiménez, J.M., Proenza, J.A., Gervilla, F., Melgarejo, J.C., Blanco-Moreno, J. A., Ruiz-Sánchez, R., Griffin, W.L., 2011. High-Cr and high-Al chromitites from the Sagua de Tánamo district, Mayarí-Cristal ophiolitic Massif (eastern Cuba): constraints on their origin from mineralogy and geochemistry of chromian spinel and platinumgroup elements. Lithos 125, 101–121.

Hart, S.R., Hauri, E.H., Oschmann, L.A., Whitehead, J.A., 1992. Mantle plumes and entrainment: isotope evidence. Science 256, 517–520.

Helmy, H.M., El Mahallawi, M.M., 2003. Gabbro Akarem mafic-ultramafic complex, Eastern Desert, Egypt: a late precambrian analogue of Alaskan-type complexes. Mineral. Petrol. 77, 85e108.

Helmy, H.M., Abd El-Rahman, Y., Yoshikawa, M., Shibata, M., Arai, S., Kagami, H., Tamura, A., 2014. Petrology and Sm–Nd dating of the Genina Gharbia Alaskan-type complex (Egypt): insights into deep levels of Neoproterozoic island arcs. Lithos 198–199, 263–280.

Helmy, H.M., Yoshikawa, M., Shibata, T., Arai, S., Kagami, H., 2015. Sm–Nd and Rb–Srisotope geochemistry and petrology of Abu Hamamid intrusion, Eastern Desert, Egypt: an Alaskan-type complex in a back arc setting. Precambr. Res. 258, 234–246.

Huang, X.N., Li, J.H., Kusky, T.M., Chen, Z., 2004. Microstructures of the Zunhua 2.50 Ga podiform chromite, North China Craton and implications for the deformation and rheology of the Archean oceanic lithospheric mantle. In: Kusky, T.M. (Ed.), Precambrian Ophiolites and Related Rocks, Developments in Precambrian Geology, vol. 13. Elsevier, Amsterdam, pp. 321–337.

Irvine, T.N., 1967. Chromian spinel as a petrogenetic indicator: Part 2. Petrologic applications. Can. J. Earth Sci. 4, 71–103.

Ishii, T., Robinson, P.T., Maekawa, H., Fiske, R., 1992. Petrological studies of peridotites from diapiric serpentinite seamounts in the Izu-Ogasawara-Mariana forearc, Leg 125. In: Fryer, P., Pearce, J.A., Stokking, L.B., et al. (Eds.), Proc O.D.P. Sci. Res. 125, pp. 445–486.

Iyer, K., Austrheim, H., John, T., Jamtveit, B., 2008. Serpentinization of the oceanic lithosphere and some geochemical consequences: constraints from the Lekaophiolite complex, Norway. Chem. Geol. 249, 66–90.

Jan, M.Q., Khan, M.A., Windley, B.F., 1992. Exsolution in Al-Cr-Fe^{3+}-rich spinels from the Chilas mafic-ultramafic complex, Pakistan. Am. Miner. 77, 1074–1079.

Ismail, S.K., Arai, S., Ahmed, A.H., Shimizu, Y., 2009. Chromitite and peridotite from Rayat, northeastern Iraq, as fragments of a Tethyan ophiolite. J. Island Arc 18, 175–183.

Johnson, L.E., Fryer, P., 1990. The first evidence of MORB-like lavas from the outer Mariana forearc: geochemistry, petrography and tectonic implications. Earth Planet. Sci. Lett. 100, 304–316.

Johnson, P.R., 1998. The Structural Geology of the Samran-Shayban Area. Kingdom of Saudi Arabia: Saudi Arabian Deputy Ministry for Mineral Resources Open File Report USGS-OF-98-2, p. 45.

Kamenetsky, V., Crawford, A.J., Meffre, S., 2001. Factors controlling chemistry of magmatic spinel: an empirical study of associated olivine, Cr-spinel and melt inclusions from primitive rocks. J. Petrol. 42, 655–671.

Kattan, F.H., 1983. Petrology and Geochemistry of the Tuluhah Belt, North East Arabian Shield (M.S. thesis). King Abdulaziz University, Jiddah.

Khedr, M.Z., Arai, S., 2013. Origin of Neoproterozoic ophiolitic peridotites in south Eastern Desert, Egypt, constrained from primary mantle mineral chemistry. Mineral. Petrol. 107, 807–828.

Krause, J., Brugmann, G.E., Pushkarev, E.V., 2007. Accessory and rock forming minerals monitoring the evolution of zoned mafic–ultramafic complexes in the central Ural mountains. Lithos 95, 19–42.

Kusky, T.M., Li, J.H., Glass, A., Huang, X.N., 2004. Origin and emplacement of Archean ophiolites of the Central Orogenic belt, North China craton. In: Kusky, T.M. (Ed.), Precambrian Ophiolites and Related Rocks, Developments in Precambrian Geology, vol. 13. Elsevier, Amsterdam, pp. 223–274.

Le Mee, L., Girardeau, J., Monnier, C., 2004. Mantle segmentation along the Oman ophiolite fossil mid-ocean ridge. Nature 432, 167–172.

Leblanc, M., 1991. Platinum-group elements and gold in ophiolitic complexes: distribution and fractionation from mantle to oceanic floor. In: Peters, T. et al. (Eds.), Ophiolite Genesis and Evolution of the Oceanic Lithosphere. Kluwer, Dordrecht, The Netherlands, pp. 231–260.

Leblanc, M., Ceuleneer, G., 1992. Chromite crystallization in a multicellular magma flow: evidence from a chromitite dikes in the Oman ophiolite. Lithos 27, 231–257.

Li, J., Kusky, T.M., Huang, X., 2002. Archean podiform chromitites and mantle tectonites in ophiolitic mélange, North China Craton: a record of early oceanic mantle processes. GSA Today, 4–11.

Liipo, J., Vuollo, J., Nykänen, V., Piirainen, T., Pekkarinen, L., Tuokko, I., 1995. Chromites from the early Proterozoic Outokumpu-Jormua ophiolite belt: a comparison with chromites from Mesozoic ophiolites. Lithos 36, 15–27.

Liu, C.-Z., Snow, J.E., Hellebrand, E., Brügmann, G., von der Handt, A., Büchl, A., Hofmann, A.W., 2008. Ancient, highly heterogeneous mantle beneath Gakkel ridge, Arctic Ocean. Nature 452, 311–315.

Luguet, A., Lorand, J.-P., Seyler, M., 2003. Sulfide petrology and highly siderophile element geochemistry of abyssal peridotites: a coupled study of samples from the Kane Fracture Zone (45°W 23°20N, MARK Area, Atlantic Ocean). Geochim. Cosmochim. Acta 67, 1553–1570.

Matveev, S., Ballhaus, C., 2002. Origin of podiform chromite deposits. Earth Planet. Sci. Lett. 203, 235–243.

Maurel, C., Maurel, P., 1982. Étude expérimentale de la distribution de l'aluminium entre bain silicaté basique et spinelle chromifère. Implications pétrogénétiques: teneur en chrome des spinelles. Minéral B 105, 197–202.

Melcher, F., Grum, W., Simon, G., Thalhammer, T.V., Stumpfl, E.F., 1997. Petrogenesis of the giant ophiolitic chromite deposits of Kempirsai, Kazakhstan: a study of solid and fluid inclusions in chromite. J. Petrol. 38, 1419–1458.

Mitchell, R.H., Keays, R.R., 1981. Abundance and distribution of gold, palladium and iridium in some spinel and garnet lherzolites: implications for the nature and origin of precious metal-rich intergranular components in the upper mantle. Geochim. Cosmochim. Acta 45, 2425–2442.

Miura, M., Arai, S., Ahmed, A.H., Mizukami, T., Okuno, M., Yamamoto, S., 2012. Podiform chromitite classification revisited: a comparison of discordant and concordant chromitite pods from Wadi Hilti, northern Oman ophiolite. J. Asian Earth Sci. 59, 52–61.

Mondal, S.K., Ripley, E.M., Li, C., Frei, R., 2006. The genesis of Archaean chromitites from the Nuasahi and Sukinda massifs in the sighbum Craton, India. Precambr. Res. 148, 45–66.

Moores, E.M., 1982. Origin and emplacement of ophiolites. Rev. Geophys. Space Phys. 20, 735–760.

Moores, E.M., Kellogg, L.H., Dilek, Y., 2000. Tethyan ophiolites, mantle convection, and tectonic 'historical contingency'; a resolution of the 'ophiolite conundrum'. In: Dilek, Y., Moores, E., Elthon, D., Nicolas, A. (Eds.), Ophiolites and Oceanic

Crust; New Insights from Field Studies and the Ocean Drilling Program: Special Paper, vol. 349. Geol. Soc. America, pp. 3–12.
Naldrett, A.J., 1981. Platinum-group element deposits. In: Cabri, L.J. (Ed.), PGE Mineralogy, Geology, Recovery, vol. 23. Canadian Institute of Mining and Metallurgical Publication, pp. 197–231 (Special volume).
Naldrett, A.J., Duke, J.M., 1980. Platinum metals in magmatic sulfide ores. Science 208, 1417–1424.
Nassief, M.O., Macdonald, R., Gass, I.G., 1984. The Jabal Thurwah upper Proterozoic ophiolite complex, western Saudi Arabia. J. Geol. Soc. Lond. 141, 537–546.
Neary, C.R., Brown, M., 1979. Chromites from A1 Ays complex, Saudi Arabia and the Semail complex. In: Al Shanti, A.M.S. (Ed.), Evolution and Mineralization of the Arabian Shield. Int. Assoc. Geol. Bull., pp. 193–205.
Ordóñez-Calderón, J.C., Polat, A., Fryer, B., Gagnon, J.E., Raith, J.G., Appel, P.W.U., 2008. Evidence for HFSE and REE mobility during calc-silicate metasomatism, Mesoarchaean (~3075 Ma) Ivisaartoq greenstone belt, southern west Greenland. Precambr. Res. 161, 317–340.
Ozawa, K., 1983. Relationships between tectonite and cumulate in ophiolites: the miyamori ultramafic complex, Kitakami Mountains, northeast Japan. Lithos 16, 1–16.
Page, N.J., Talkington, R.W., 1984. Palladium, platinum, rhodium, ruthenium, and iridium in peridotites and chromitites from ophiolite complexes in Newfoundland. Can. Miner. 22, 137–149.
Parkinson, I.J., Pearce, J.A., 1998. Peridotites of the Izu-Bonin-Mariana forearc (ODP Leg 125) evidence for mantle melting andmelt–mantle interactions in a suprasubduction zone setting. J. Petrol. 39, 1577–1618.
Pearce, J.A., Barker, P.F., Edwards, S.J., Parkinson, I.J., Leat, P.T., 2000. Geochemistry and tectonic significance of peridotites from the South Sandwich arc basin system, south Atlantic. Contrib. Mineral. Petrol. 139, 36–53.
Peltonen, P., Kontinen, A., Huhma, H., 1998. Petrogenesis of the mantle sequence of the Jormua Ophiolite (Finland): melt migration in the upper mantle during Palaeoproterozoic continental break-up. J. Petrol. 39, 297–329.
Peltonen, P., Kontinen, A., 2004. The Jormua ophiolite: a mafic-ultramafic complex from an ancient ocean-continent transition zone. In: Kusky, T.M. (Ed.), Precambrian Ophiolites and Related Rocks, Developments in Precambrian Geology, vol. 13. Elsevier, Amsterdam, pp. 35–71.
Polat, A., Appel, P.W.U., Frei, R., Pan, Y., Dilek, Y., Ordonez Caldeeron, J.C., Fryer, B., Raith, J.G., 2007. Field and geochemical characteristics of the Mesoarchean (~3075 Ma) Ivisaartoq greenstone belt, southern west Greenland: evidence for seafloor hydrothermal alteration in a supra-subduction oceanic crust. Gondwana Res. 11, 69–91.
Quick, J.E., 1990. Geology and origin of late Proterozoic Darb Zubaydah ophiolite, Kingdom of Saudi Arabia. Geol. Soc. Am. Bull. 102, 1007–1020.
Roberts, S., Neary, C., 1993. Petrogenesis of ophiolitic chromitite. In: Prichard, H.M., Alabaster, T., Harris, N.B.W., Neary, C.R. (Eds.), Magmatic Processes and Plate Tectonics, vol. 76. Geol. Soc. Spec. Publ., pp. 257–272.
Roeder, P.L., 1994. Chromite. from the Fiery rain of chondrules to the Kilauea iki lava lake. Can. Mineral. 32, 729–746.
Rollinson, H., 2008. The geochemistry of mantle chromitites from the northern part of the Oman ophiolite: inferred parental melt compositions. Contrib. Mineral. Petrol. 156, 273–288.
Stern, R.J., Johnson, P.R., Kröner, A., Yibas, B., 2004. Neoproterozoic ophiolites of the Arabian-Nubian Shield. In: Kusky, T.M. (Ed.), Precambrian Ophiolites and Related Rocks: Development of Precambrian. Geology 13, pp. 95–128.
Stockman, H.W., Hlava, P.F., 1984. Platinum-group minerals in Alpine chromitites from southwestern Oregon. Econ. Geol. 79, 491–508.
Stoeser, D.B., Camp, V.E., 1985. Pan-African microplate accretion in the Arabian shield. Geol. Soc. Am. Bull. 96, 817–826.
Stoeser, D.B., Stacey, J.S., 1988. Evolution, U-Pb geochronology and isotope geology of the Pan-African Nabitah orogenic belt of the Saudi Arabian Shield. In: El-Gaby, S., Greiling, R.O. (Eds.), The Pan african belt of Northeast Africa and Adjacent Areas. Vieweg Braunschweig, Wiesbaden, pp. 227–288.
McDonough, W.F., Sun, S.S., 1989. Chemical and isotopic systematics of oceanic basalts: implications for mantle composition and processes. In: Saunders, A.D., Norry, M.J. (Eds.), Magmatism in the Ocean Basins, vol. 42. Geol. Soc. Spec. Publ., London, pp. 313–345.
Torres-Ruiz, J., Garuti, G., Gazzotti, M., Gervilla, F., Fenollhach-Alí, P., 1996. Platinum-group minerals in chromitites from the Ojén lherzolite massif (Serranía de Ronda, Betic Cordillera, southern Spain). Mineral. Petrol. 56, 25–50.
Van der Laan, S.R., Arculus, R.J., Pearce, J.A., Murton, J.B., 1992. Petrography, mineral chemistry, and phase relations of the basement boninite series of Site 786, Izu–Bonin forearc. In: Fryer, P., Pearce, J.A., Stokking, L.B. (Eds.), Proceedings of the Ocean Drilling Program, Scientific Results, vol. 125. Ocean Drilling Program, College station, TX, pp. 171–202.
Van der Veen, A.H., Maaskant, P., 1995. Chromian spinel mineralogy of the Staré Ransko gabbro-peridotite, Czech Republic, and its implications for sulfide mineralization. Miner. Deposita 30, 397–407.
Vuollo, I., Liipo, I., Nykanen, V., Piirainen, T., Pekkarinen, L., Tuokko, I., Ekdahl, E., 1995. An early Proterozoic podiform chromitite in the Outokumpu ophiolite complex, Finland. Econ. Geol. 90, 445–452.
Wilson, M., 1989. Igneous Petrogenesis. Unwin Hyman, London, p. 446.
Woods, S.A., 1987. Thermodynamic calculations of the volatility of the platinum group elements (PGE): the PGE content of fluids at magmatic temperatures. Geochim. Cosmochim. Acta 51, 3041–3050.
Zhou, M.F., Robinson, P.T., Malpas, J., Li, Z., 1996. Podiform chromitites in the Luobusa ophiolite (southern Tibet): implications for melt-rock interaction and chromite segregation in the upper mantle. J. Petrol. 37, 3–21.
Zhou, M.F., Robinson, P.T., 1997. Origin and tectonic environment of podiform chromite deposits. Econ. Geol. 92, 259–262.
Zhou, M.F., Sun, M., Keays, R.R., Kerrich, R.W., 1998. Controls on PGE distributions of podiform chromitites: a case study of high-Cr and high-Al chromitites from Chinese orogenic belts. Geochim. Cosmochim. Acta 62, 677–688.